OUKA
The University of Osaka
Institutional Knowledge Archive

Title	Studies on Local Structures and Hydrogen Absorption Characteristics of an Amorphous Rare-Earth Alloy
Author(s)	末延, 知義
Citation	大阪大学, 1994, 博士論文
Version Type	VoR
URL	https://doi.org/10.11501/3075114
rights	
Note	

The University of Osaka Institutional Knowledge Archive : OUKA

https://ir.library.osaka-u.ac.jp/

The University of Osaka

Studies on
Local Structures and Hydrogen Absorption Characteristics of an Amorphous Rare-Earth Alloy

1994

Tomoyoshi Suenobu

Department of Applied Chemistry
Faculty of Engineering
Osaka University

Studies on
Local Structures and Hydrogen Absorption Characteristics of an Amorphous Rare-Earth Alloy

(希土類系アモルファス合金の局所構造と水素吸蔵特性に関する研究)

1994

Tomoyoshi Suenobu
末延　知義

Department of Applied Chemistry
Faculty of Engineering
Osaka University

大阪大学大学院工学研究科　応用化学専攻

Preface

The work of this thesis has been carried out under the guidance of Professor Dr. Gin-ya Adachi at Department of Applied Chemistry, Faculty of Engineering, Osaka University.

The object of this thesis is to clarify the local structure of an amorphous $LaNi_5$ alloy that represents the rare-earth hydrogen storage alloy and to discover the correlation between the local structure and hydrogen absorption characteristics of this alloy.

The author hopes that the knowledge obtained in this work can contribute to further understanding of the mechanisms of hydrogen storage for the rare-earth alloy.

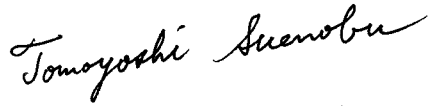

Tomoyoshi Suenobu

Department of Applied Chemistry
Faculty of Engineering
Osaka University
Yamadaoka, Suita, Osaka 565, Japan

January 1994

Contents

General Introduction ——— i

List of Publications ——— iv

Chapter 1 The Local Structure of an Amorphous $LaNi_{5.0}$ Alloy and a Comparison with a Corresponding Crystalline Alloy

1.1 Introduction ——— 1

1.2 Experimental ——— 2

1.3 Results and Discussion ——— 5

1.4 Conclusion ——— 16

Chapter 2 The Effect of Local Structures on the Hydrogen Absorption for an Amorphous $LaNi_{5.0}$ Alloy

2.1 Introduction ——— 17

2.2 Experimental ——— 18

2.3 Results and Discussion ——— 19

2.4 Conclusion ——— 32

Chapter 3 The Local Structures of an Amorphous $LaNi_{5.0}$ Alloy Having the Large Hydrogen Density

3.1 Introduction ——— 34

3.2 Experimental ——— 35

3.3 Results and Discussion ——— 36
3.4 Conclusion ——— 40

Chapter 4 Comparison of the Local Structure of the Amorphous $LaNi_{5.0}$ Alloys Prepared by Evaporation and Sputtering
4.1 Introduction ——— 41
4.2 Experimental ——— 41
4.3 Results and Discussion ——— 42
4.4 Conclusion ——— 47

Chapter 5 Correlation between the Local Structures and the Electronic States of $LaNi_5$ Alloy Hydrides
5.1 Introduction ——— 49
5.2 Calculation ——— 51
5.3 Results and Discussion ——— 53
5.4 Conclusion ——— 60

Summary ——— 61

References ——— 64

Acknowledgment ——— 67

General Introduction

Rare earth-based hydrogen storage alloys have proven to be an excellent medium for handling hydrogen because the alloys can absorb much hydrogen safely, quickly and reversibly under moderate conditions.[1-3)]

Extensive application research concerning hydrogen purification, batteries and heat pumps has been made.[4-6)] The secondary batteries using the alloys as a negative electrode material have been placed on the market on an industrial scale. On the other hand, there is very little basic knowledge about the mechanism of hydrogen absorption, because efforts related to this type of alloy have focused primarily on technical research and development.

These alloys disintegrate into fine particles of average diameter about one micron by hydrogen absorption-desorption cycles and this becomes a serious problem in its practical application.[7)] Adachi et al. have succeeded in preparing an amorphous thin film of $LaNi_{5.0}$ by a flush evaporation or magnetron RF sputtering method and the mechanical properties of these films have been studied.[6,8)] It was surprising that the alloy film did not pulverize after repeated hydrogenation process. Therefore, it was expected to be useful as a hydrogen-separating membrane instead of palladium sheet. The alloy film, however, has been known to absorb hydrogen less than a half of the amount

taken up by the crystalline bulk. [9)]

These differences of hydrogen absorption properties between the amorphous film and the crystalline bulk appear to be closely related to the structure of the alloy, so that it is necessary to obtain the detailed structural information at an atomic level.

In the present work, the author discussed to relate the hydrogen absorption characteristics of an amorphous $LaNi_5$ alloy to its microstructure.

Although numerous studies have been devoted to clarify the correlation between the structure and hydrogen absorption properties for the crystalline $LaNi_5$ alloy, [10-15)] almost nothing is known about the corresponding amorphous alloys. It is therefore important to perform structural studies of the amorphous alloy.

An amorphous material does not have the long-range order and the appearance of its unique properties depends on the short-range structure. Studies of the short-range structure on various metal-metalloid and metal-metal multicomponent amorphous alloys have been carried out using X-ray, neutron scattering techniques and EXAFS. The radial distribution function obtained from the scattering experiments described above is, however, composed of all kinds of atom-atom correlations, so that it is difficult to separate the contribution of the each correlation in the multicomponent system like the $LaNi_5$ alloy.

Structural analysis by EXAFS (Extended X-ray Absorption Fine Structure) proves to be the optimum method for analyzing the

structure of amorphous alloys because it provides detailed information about the local structure around each component atom of multicomponent samples, so that EXAFS was used to analyze the microstructure of amorphous alloys treated in this thesis.[16)]

Moreover, in order to clarify whether the local electronic states of the $LaNi_5$ alloy hydride is related to the hydrogen absorption properties of these alloy or not, we also calculated the electronic states of the alloy and its hydride using the DV-Xα method.[17)]

This thesis consists of the following five chapters.

Chapter 1 describes the local structure of the $LaNi_{5.0}$ amorphous alloy prepared by sputtering and a comparison of the structure for the amorphous alloy with that for the crystalline one.

On the basis of the structural parameters obtained, hydrogen sites in the amorphous $LaNi_{5.0}$ are discussed.

Chapter 2 refers first to changes in the local structure as the amorphous alloy became hydrogenated and then to the correlation between the change of the structure and hydrogen absorption characteristics. Furthermore, a mechanism of hydrogen absorption for the amorphous alloy is proposed.

Chapter 3 deals with the amorphous $LaNi_{5.0}$ alloy prepared by reactive sputtering. The alloy has been found to absorb much hydrogen in comparison with the alloy described in Chapter 1. The reason is considered from the stand point of the local structures.

In Chapter 4, another amorphous $LaNi_{5.0}$ alloy prepared by

an evaporation method is taken up, because the alloy exhibits almost the same hydrogen absorption characteristics as that of the alloy shown in Chapter 1. The local structures of the two alloys having mutually similar properties is discussed.

The stability of hydrogen in the metal-hydrogen system appears to originate from the electronic states of the small local region of the system consisting of hydrogen atom and its surrounding metals. Chapter 5 gives the results of our non-empirical calculation of electronic states of $LaNi_5$ hydrides by the DV-Xα method using cluster models of the sites occupied by hydrogen atoms.

List of Publications

1. Extended X-ray Absorption Fine Structure Studies on Local Structure in Amorphous $LaNi_{5.0}$ Films

   Tomoyoshi Suenobu, Hiroki Sakaguchi, Takaharu Tsuji, Hiroyoshi Kanai, Satohiro Yoshida and Gin-ya Adachi

   Bull. Chem. Soc. Jpn., **64**, 3522(1991).

2. Studies on Local Structure in Hydrogenated Amorphous $LaNi_{5.0}$ Films Using X-ray Absorption Fine Structure

   Tomoyoshi Suenobu, Hiroki Sakaguchi, Gin-ya Adachi, Hiroyoshi Kanai and Satohiro Yoshida

   J. Alloys Comp., **190**, 273(1993).

3. X-ray Absorption Fine Structure Studies on an Amorphous $LaNi_{5.0}$ Film Prepared by Reactive Sputtering

Hiroki Sakaguchi, Tomoyoshi Suenobu, Tetsuji Tsujimoto, Kiyoaki Moriuchi, Hiroyoshi Kanai, Satohiro Yoshida and Gin-ya Adachi

Jpn. J. Appl. Phys., Suppl. **32-2**, 679(1993).

4. Structural Studies on Amorphous $LaNi_{5.0}$ Films as Prepared in Different Methods

Tomoyoshi Suenobu, Hiroki Sakaguchi, Kazuhiro Nishioka, Hiroyoshi Kanai, Satohiro Yoshida and Gin-ya Adachi

Jpn. J. Appl. Phys., Suppl. **32-2**, 682(1993).

5. Correlation between the Electronic Structure and Hydrogen Absorption Characteristics in α-phase $LaNi_5$ Hydrides

Tomoyoshi Suenobu, Isao Tanaka, Hirohiko Adachi and Gin-ya Adachi

J. Am. Chem. Soc., in contribution.

List of Supplementary Publication

1. Hydrogen permeability for oxide-metal multilayered films

Hiroki Sakaguchi, Hiroo Shirai, Kazuhiro Nishioka , Tomoyoshi Suenobu, Hidenori Tanaka and Gin-ya Adachi

J. Alloys Comp., **185**, 295(1992).

Chapter 1

The Local Structure of an Amorphous $LaNi_{5.0}$ Alloy and a Comparison with a Corresponding Crystalline Alloy

1.1 Introduction

The physical and chemical properties of amorphous $LaNi_5$ films have been found to be much different from those of the crystalline sample.[8,9,18,19] The amorphous $LaNi_5$ film has been known not to pulverize after repeated hydrogenation-dehydrogenation cycling, and absorbs hydrogen less than a half of the amount taken up by the crystalline bulk as shown in Fig.1-1.[5,9]

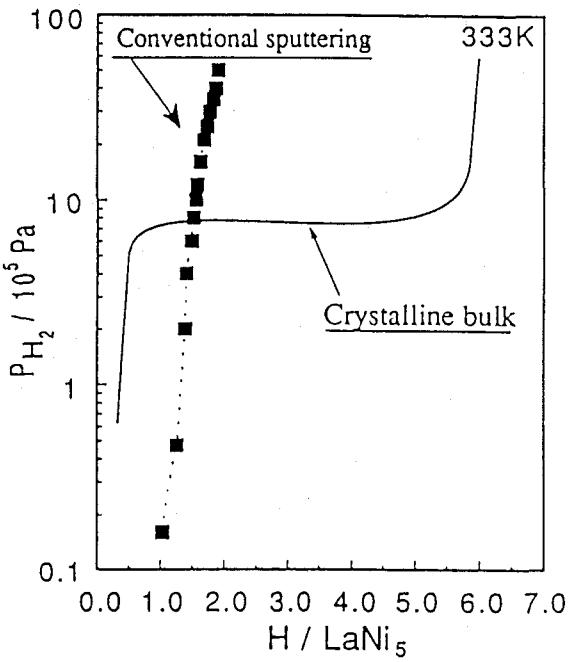

Fig. 1-1. Hydrogen absorption properties of the $LaNi_{5.0}$ crystalline bulk and the amorphous film.

These differences of properties appear to be closely related to the structure of the films, so that it is necessary to obtain the detailed structural information.

In this chapter, the local structure around La and Ni atoms in the amorphous $LaNi_{5.0}$ films is clarified by means of EXAFS, and the results are compared with those in the crystalline sample. The relationship between the structure and the hydrogen absorption characteristics is discussed.

1.2 Experimental

$LaNi_{5.0}$ amorphous films(ca. 1 μm thick which was determined by direct observation of the cross section of the sample using a scanning electron microscope.) were deposited on a polyimide membrane(Kapton, 40 μm thick, Toray - du Pont Co., Ltd.) at room temperature by using sputtering method. For the sputtering, parameters of 0.395-Pa Argon pressure(99.999 %) and a radio-frequency generating power of 400 W were employed for all sputtered samples. The sputtering target consisted of a disk in which 98 % of the surface area is $LaNi_{4.8}$(33.0 wt% La, 66.8 wt% Ni) and 2 % is $LaNi_{3.0}$. The La-Ni alloys were supplied by Santoku Metal Industry, Kobe, Japan. X-ray diffraction measurements were made to verify the amorphous state. Their homogeneity and stoichiometry were checked by means of X-ray fluorescent spectroscopy and X-ray photoelectron spectroscopy.

The films precisely having a composition of $LaNi_{5.0}$ were used for the EXAFS measurements. The $LaNi_{5.0}$ crystalline powder and commercially available Ni foil(5 μm thick, 99.98 % pure, The Japan Lamp Industries) were used as reference materials. The crystalline $LaNi_{5.0}$ alloy film with a crystallinity of 80 % was prepared on a stainless-steel substrate at 530K by sputtering. The film was peeled from the substrate with an adhesive tape, and the resulting film was applied to the EXAFS measurements. The crystallinity of the film was determined from the heat of crystallization which was estimated by the differential scanning calorimetry(DSC).[9)]

The measurement of X-ray absorption spectra(XAS) were performed by means of synchrotron radiation employing the EXAFS facilities of BL-7C of the Photon Factory in the National Laboratory for High-Energy Physics, Tsukuba, Japan. An Si(111) double crystal monochromator was used to monochromatize the X-rays from a 2.5-GeV positron storage ring. The ring current was between 350.5 and 246.9 mA. EXAFS spectra were collected at the Ni K- and La L_{III}-edges. The focusing mirror was used to reduce higher harmonics at the La edge. Energy resolution of 1.4 eV can be achieved at the Ni K-edge(8331.7 eV) when a source-size is not considered. The incident and transmitted X-ray beam intensities, namely I_0 and I, were measured using two ionization chambers. The detector gases introduced to the I_0 and I chambers were 100% pure N_2 gas and Ar(25%)-N_2(75%) gas mixture respectively in

measuring Ni K-edge XAS, while in measuring La L_{III}-edge XAS, He(90%)-N_2(10%) gas mixture and 100% pure N_2 gas were used.The total thickness of the $LaNi_{5.0}$ films used for the X-ray absorption measurements were about 35 and 20 μm for the La and Ni edges respectively. All the XAS data were obtained at 220 K. Analyses of the EXAFS data were performed with a "KABO" program in the FACOM M382 computer system at the Data Processing Center, Kyoto University, Japan.[20)]

The photon energy was calibrated by the characteristic inflection point at the edge of the absorption spectrum of the standard Ni foil(5 μm thick, 8331.7 eV). The EXAFS oscillatory part $\chi(E)$ above the absorption edge was extracted from the XAS data using a simple equation of $A/E^{2.75}$ instead of Victoreen formula and normalized as described elsewhere.[20-22)] The photoelectron wave vector k is related to the photon energy E expressed by $k=2\pi[2m(E-E_0)]^{1/2}/h$, where m is mass of an electron, h, Planck's constant, E_0, the threshold energy of the absorption edge. E_0 was determined as $E_{inf}+\Delta E$, where E_{inf} was the inflection point where the differential coefficient of the spectrum near the absorption edge is maximum and ΔE was allowed to be various fixed values. Reconstruction of the crystalline $LaNi_{5.0}$ spectra can only be achieved using +4.5eV as ΔE at Ni K-edge and +4.0eV at La L_{III}-edge. Subsequently, $E_0(=E_{inf}+\Delta E)$ was determined with these ΔE values for the amorphous and 80% crystallinity films. Fourier transforms are

taken over the range of 3.3-14.0 $Å^{-1}$ and 4.0-9.2 $Å^{-1}$ for the Ni and La edges respectively to obtain the radial structure function(RSF). In order to obtain the bond distance and the coordination number, the main peaks(Ni;1.6-2.7 Å, La; 2.4-3.4 Å) were Fourier filtered into the k space, where the inverse Fourier transform was analyzed by the single scattering formula of Stern et al.[23-25] The resulting filtered EXAFS was fitted to the formula of Stern et al., with three variables, namely, B(=N×S ; N, true coordination number, S, damping factor which was evaluated from the coordination number of the Ni foil.[26], apparent coordination number, L, interatomic distance, and σ^2, Debye-Waller factor by means of the nonlinear least square curve-fitting method.[27] Theoretical phase shifts and backscattering amplitudes of Teo and Lee are used in the curve fitting analyses.[28,29] As obtained in general EXAFS measurements,[30,31] the errors in the parameters of B and L were determined as the ranges within which the R value changes by a factor of 2 from the minimum value, with the other parameters held fixed, where R is a reliability factor.

1.3 Results and Discussion

Figure 1-2 illustrates XANES spectra on the Ni k-edge for the Ni foil, the $LaNi_{5.0}$ crystalline bulk and the $LaNi_{5.0}$ amorphous

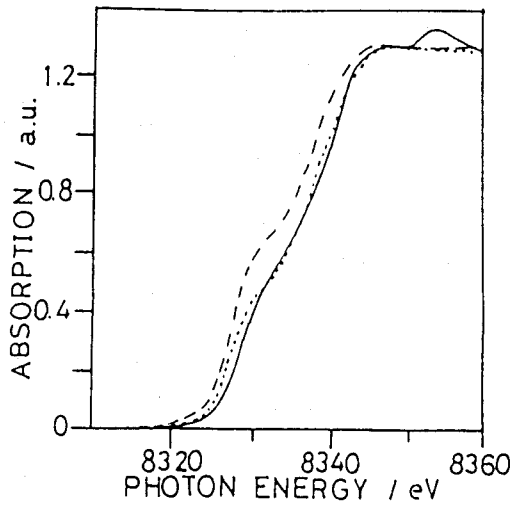

Fig. 1-2. Ni K-edge XANES spectra for $LaNi_{5.0}$.
——— :Ni foil, ------:$LaNi_{5.0}$ crystalline bulk
····· :$LaNi_{5.0}$ amorphous sputtered film

sputtered film. The absorption edge for the $LaNi_5$ crystalline bulk shifted about 1.5 eV to the lower energy side compared with that for the Ni foil due to the narrowing of the Ni 3d-band caused by the charge transfer from the 5d-band of La, which has smaller electronegativity than Ni, to the Ni 3d-band. As for the $LaNi_{5.0}$ amorphous film, the energy position of absorption edge was higher than that for the crystalline bulk. However, no difference of the energy position of absorption edge was observed between the amorphous $LaNi_{5.0}$ film and the Ni foil. This is because the degree of energy transfer from La to Ni for the amorphous film is lower than that for the crystalline bulk.

Figures 1-3 and 1-4 show the k^3-weighted EXAFS spectra at the Ni K- and La L_{III}-edges in the sputtered amorphous $LaNi_{5.0}$ films and the 80 % crystallinity film. The amplitude of the EXAFS oscillations for the amorphous film was smaller than that for the

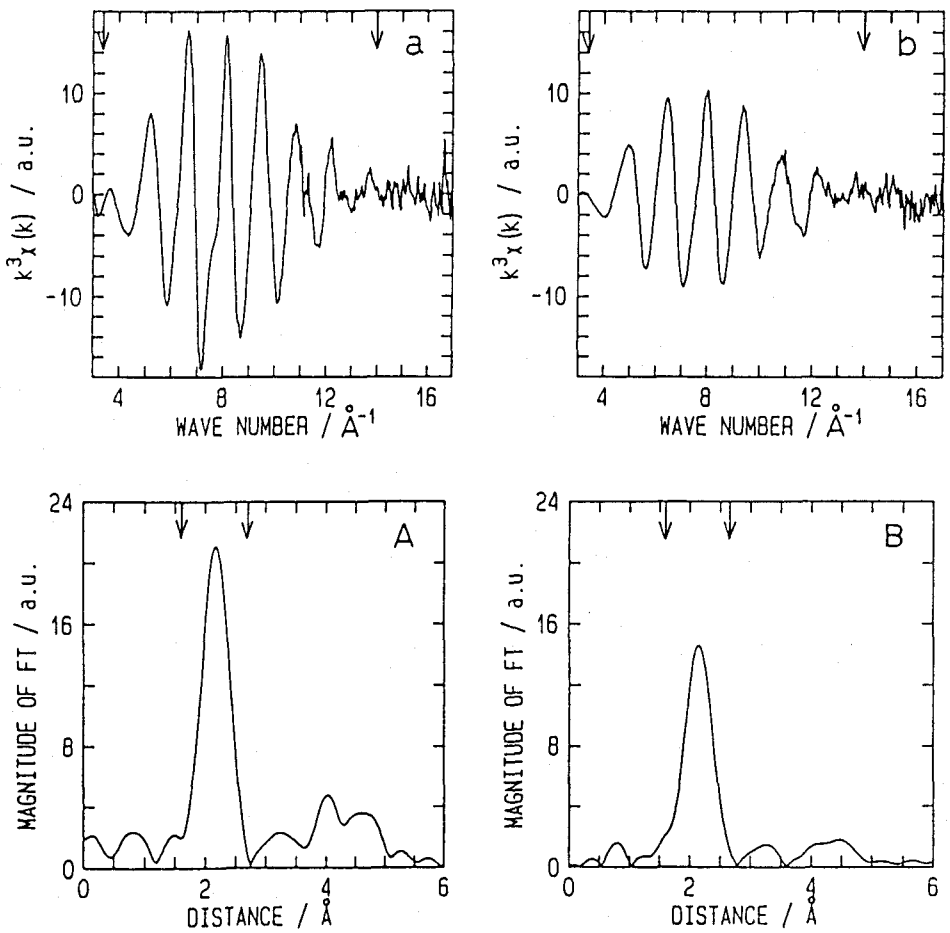

Fig. 1-3. Ni K-edge k^3-weighted EXAFS spectra(a-b) and magnitudes of their Fourier transforms(A-B), in the 80% crystallinity(a,A) and the amorphous sputtered(b,B) $LaNi_{5.0}$ films. (Arrows (↓) illustrated in the figures indicate the range for Fourier transforms or back Fourier transforms.)

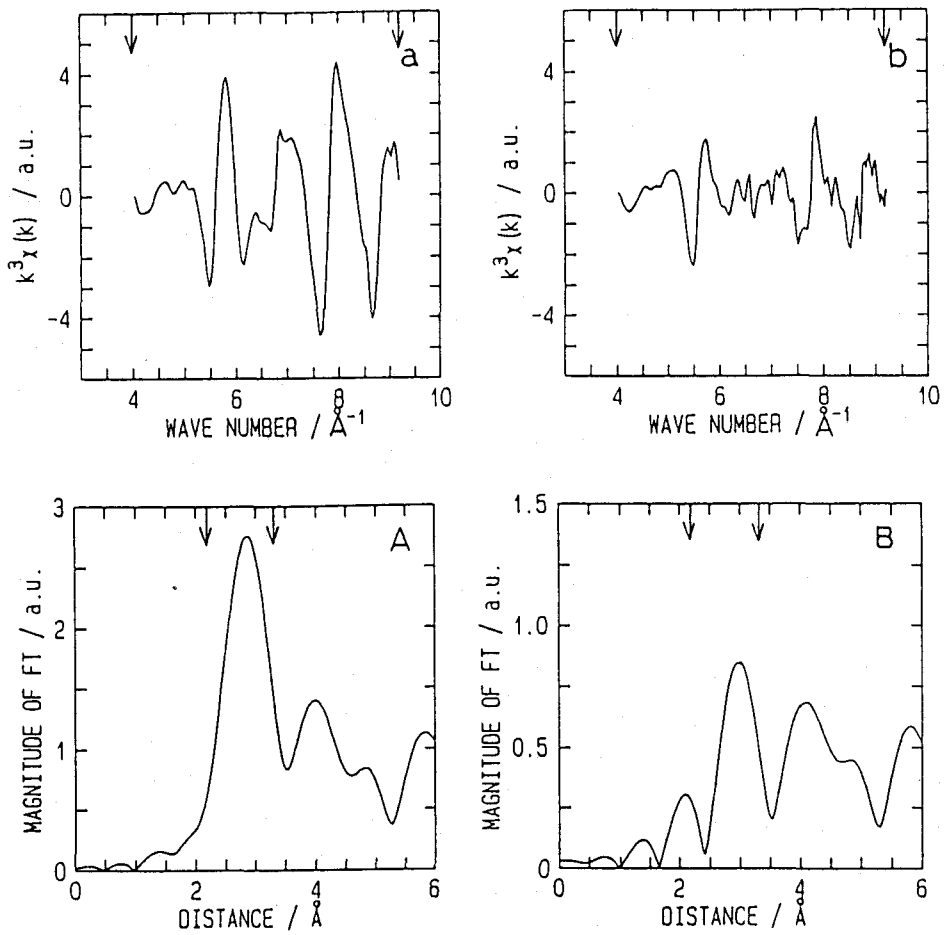

Fig. 1-4. La L_{III}-edge k^3-weighted EXAFS spectra(a-b) and magnitudes of their Fourier transforms(A-B), in the 80% crystallinity(a,A) and the amorphous sputtered(b,B) $LaNi_{5.0}$ films.

crystalline film with a crystallinity of 80 %. The damping of EXAFS oscillation for the amorphous film seems not to be caused by the decrease in the coordination number, but by the larger static disorder which increases the Debye-Waller factor.

The magnitudes of the Fourier transforms obtained by a Fourier analysis of the EXAFS data in these films are also shown in Figs. 1-3 and 1-4. A large peak appeared in these samples on the Ni edge at about 2 Å corresponding to mainly the Ni-Ni and partially Ni-La distance, while on the La edge at about 3 Å corresponding to the La-Ni distance. The profiles of transforms in the sputtered amorphous films show resemblance to that in the 80 % crystallinity film, so that it was suggested that the local structures around central Ni and La atoms for the amorphous $LaNi_5$ were similar to those for the crystalline one. The weak intensity of the main peak for the amorphous films was observed on both two edges due to the larger static disorder.

The results of the curve fitting analysis on the Ni edge are presented in Table 1-1. As for the shortest Ni-Ni(Ni_I-Ni_{II}) pairs with an interatomic distance of 2.461 Å, the coordination number around Ni_I atoms(CN:6) is different from that around Ni_{II} atoms(CN:4), since there are two kinds of Ni atoms(Ni_I and Ni_{II}) having the different symmetry in $LaNi_5$. Therefore, the coordination number for the pairs was estimated with considering the proportion of the number of each Ni atoms in a unit cell. The

Table 1-1. Structural parameters at the Ni K-edge for $LaNi_{5.0}$ alloys.

Centrtal atom	Crystalline bulk N [XRD]	L(Å)	σ^2(Å$^2\times10^{-3}$)	R	80% crystallinity sputtered film N	L(Å)	σ^2(Å$^2\times10^{-3}$)	R
Ni	4.8Ni	2.45±0.01	5.2		5.0±0.6Ni	2.46±0.01	5.2	
	4Ni	2.51±0.01	6.0	3.1×10^{-3}	4.5±1.1Ni	2.56±0.01	8.7	6.2×10^{-3}
	3La	2.89±0.06	8.5		1.4±1.2La	2.90±0.06	8.8	

Centrtal atom	Amorphous sputtered film N	L(Å)	σ^2(Å$^2\times10^{-3}$)	R
Ni	4.6±0.5Ni	2.46±0.01	6.8	
	3.5±0.9Ni	2.57±0.02	13.2	4.8×10^{-3}
	1.7±1.4La	2.92±0.08	14.6	

L, interatomic distance; N, real coordination number; B, apparent coordination number;
σ, Debye-Waller factor; $R=[\{\Sigma_k(\chi_{obs}(k)-\chi_{calc}(k))^2\}/\{\Sigma_k\chi_{obs}(k)\}^2]^{1/2}$

Table 1-2. Structural parameters at the La L_{III}-edge for $LaNi_{5.0}$ alloys.

Centrtal atom	Crystalline bulk N [XRD]	L(Å)	σ^2(Å$^2\times10^{-2}$)	R	80% crystallinity sputtered film N	L(Å)	σ^2(Å$^2\times10^{-2}$)	R
La	6Ni	2.91±0.03	2.1		1.7±0.1Ni	2.96±0.02	2.0	
	12Ni	3.28±0.01	1.1	1.1×10^{-3}	3.8±0.1Ni	3.28±0.01	1.4	9.8×10^{-4}

Centrtal atom	Amorphous sputtered film N	L(Å)	σ^2(Å$^2\times10^{-2}$)	R
La	1.3±0.1Ni	3.01±0.01	2.1	
	2.8±0.2Ni	3.27±0.01	2.1	6.6×10^{-3}

L, interatomic distance; N, real coordination number; B, apparent coordination number; σ, Debye-Waller factor; $R=[\{\Sigma_k(\chi_{obs}(k)-\chi_{calc}(k))^2\}/\{\Sigma_k\chi_{obs}(k)\}^2]^{1/2}$

calculation was performed with the following equation, (6x2+4x3)/5=4.8.

A fit of the oscillations above the Ni edge was attempted for the crystalline $LaNi_5$ bulk with one shell of Ni atoms. The resulting interatomic distance of the Ni-Ni pair, 2.475 Å, was intermediate between the shortest distance, 2.461 Å, and the second shortest distance, 2.507 Å, which are obtained from XRD analyses,[32] so that it was suggested that the large peak appeared at about 2 Å in the RSF consisted of more than two subshells. When the curve fitting was performed with two subshells of Ni atoms at two different distances from the central atom, the distances of the two Ni-Ni pairs were 2.461 Å and 2.501 Å respectively. Although these distances were fairly fitted with those estimated from the XRD analyses, the reliability (R) and Debye-Waller (σ^2) factors were still large. Therefore, the interatomic distances were determined by adding one subshell of La atoms at a larger distance(2.89 Å) to the two subshells of Ni atoms. The combination of these three subshells could simulate the spectrum, since both R and σ^2 factors were smaller than the result obtained from the curve fitting with two Ni subshells. For the crystalline bulk, the coordination number obtained with EXAFS is not listed in the table because the XAS was not satisfactory.

The structural parameters of the amorphous film were similar

to those of the crystalline bulk though there is a slight difference in the interatomic distance. This indicates that the sites accommodated with hydrogen atoms in the amorphous film were analogous to those in the crystalline bulk. The distances of second Ni-Ni pairs were found to increase about 0.06 Å for the amorphous films in comparison with those for the crystalline bulk. The parameters of interatomic distances for the amorphous sputtered film were slightly different from those for the crystalline film which has a crystallinity of 80 %.

The structural parameters for the La edge are summarized in Table 1-2. The coordination number listed in the table is a tentative value because no adequate result for the $LaNi_{5.0}$ powder as a reference material was obtained from the EXAFS analysis due to inhomogeneities of the particle size in the sample layer.

Lanthanum atoms in the crystalline bulk are known to be coordinated by two kinds of nickel atoms(La-Ni_I; ca. 2.9 Å, La-Ni_{II}; ca. 3.2 Å). For the curve fitting analyses on La-L_{III} edges, the inverse Fourier transform of calculated EXAFS with these two subshells of La-Ni pairs fairly agree with that of experimental EXAFS. The ca. 0.1 Å lengthening of La-Ni_I pairs were found for the amorphous films in comparison with those for the crystalline bulk. On the Ni K edge, however, it was not possible to evaluate the differences of Ni_I-La distances between the amorphous film and the crystalline bulk because of large uncertainties in these

parameters due to small contribution of the Ni_I-La third subshell to the first nearest neighbor shell consisted of Ni_I-Ni_{II}, Ni_{II}-Ni_{II}, and Ni_I-La subshells.

$LaNi_5$ crystallizes with a hexagonal $CaCu_5$-type structure (P6/mmm space group). The structure consists of two alternating types of plane, the basal plane being consisted of lanthanum and nickel atoms(Ni_I), while the z=1/2 plane being consisted of only nickel atoms(Ni_{II}). There are at least three models used to describe the structure of $LaNi_5$ hydride.[11,12,33] We employed to the model reported by Lartigue et al.,[12] because the refinement of neutron powder diffraction data for their analyses gave better reliability

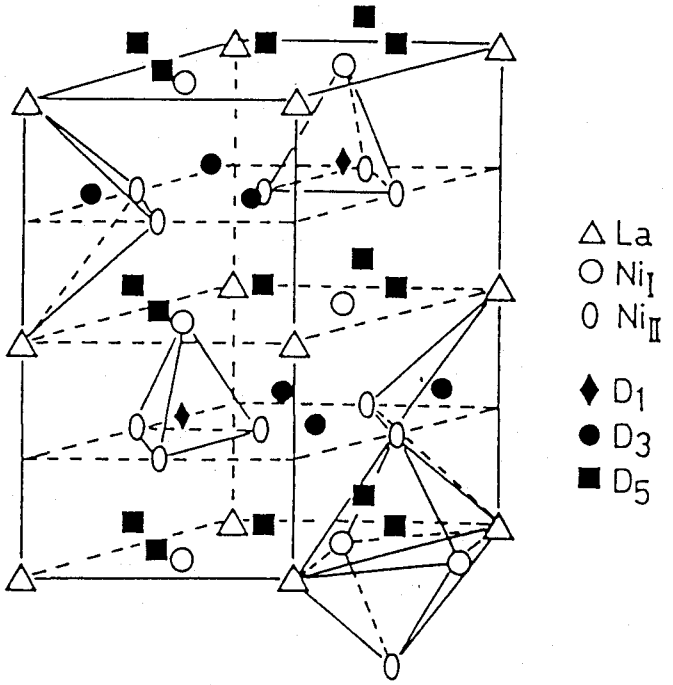

Fig. 1-5. Structure of the hypothetical fully ordered $LaNi_5D_7$ phase involving three types of sites occupied with hydrogen.

factors. According to the model ($P6_3mc$ space group), as shown in Fig. 1-5, there are three types of sites (D1, D3 and D5 sites) occupied with hydrogen or deuterium atoms for the crystalline bulk. On the D1 site(2b), hydrogen atoms are found nearly at the center of the Ni_4 tetrahedra($3Ni_I+1Ni_{II}$). On 6c sites, D3 and D5 atoms are displaced by about 0.4 Å from the center of both the tetrahedra[two lanthanum and two nickel atoms(Ni_{II})], and octahedra[two lanthanum and four nickel atoms($2Ni_I+2Ni_{II}$)]. On the local structures obtained from the EXAFS analyses, the La and Ni environments do not vary much from the crystalline bulk to the amorphous film, as was suggested by the fact that the Fourier transforms do not change much on the La and Ni edges. Moreover, the Ni-Ni and La-Ni distributions in the amorphous film still have some resemblance to the crystalline bulk, so that the three types of hydrogen sites(D1, D3 and D5) appear to exist in the amorphous film as well as the crystalline bulk. As mentioned above, however, the Ni_{II}-Ni_{II} and La-Ni_I distances were lengthened compared with those for the crystalline bulk, consequently, a part of these three hydrogen sites existed in the crystalline bulk become somewhat distorted. The Debye-Waller factor, σ^2, of each atom-atom pair in Table 1-1 and 1-2 appears to increase in the amorphous film as compared with the crystalline bulk. This indicates the increase in dispersion of the interatomic distances and, therefore, the existence of highly distorted hydrogen sites. Since the hydrogen atoms

appears to be difficult to be stably located in the sites highly distorted, the amount of hydrogen taken up by the amorphous $LaNi_{5.0}$ is smaller than that by the crystalline one.

1.4 Conclusion

The local structures around La and Ni atoms in amorphous $LaNi_5$ films have been clarified with EXAFS. The distortion of three kinds of sites which hydrogen atoms are considered to occupy was observed in the amorphous films due to the lengthening of interatomic distances in the Ni-Ni and La-Ni pairs. The large fluctuation in the size of hydrogen sites was also found to exist in the amorphous film in comparison with the crystalline bulk. If the hydrogen atoms become difficult to be stably located in the sites highly distorted, the hydrogen content in the amorphous $LaNi_{5.0}$ would be smaller than that in the crystalline one.

Chapter 2

The Effect of Local Structures on the Hydrogen Absorption for an Amorphous $LaNi_{5.0}$ Alloy

2.1 Introduction

It has been revealed that amorphous $LaNi_{5.0}$ Films do not disintegrate into fine particles after repeated hydrogen absorption-desorption cycles and absorb hydrogen less than a half of the amount taken up by the crystalline bulk.[9] The properties appear to be certainly related to structural differences between the amorphous and crystalline alloys.

In Chapter 1 associated with the amorphous $LaNi_5$ films using extended X-ray absorption fine structure (EXAFS), the increase in the interatomic distance and Debye-Waller factor was observed in the amorphous film, though the environment of Ni and La atoms in the amorphous film resembled that in the crystalline bulk, so that a part of hydrogen sites in the amorphous film appear to be highly distorted in comparison with those in the crystalline bulk.

In this chapter, we have investigated the change of local structures around La and Ni atoms in the amorphous films with increasing hydrogen concentration by means of EXAFS, and discussed the relationship between the local structure and the hydrogen absorption characteristics.

2.2 Experimental

The $LaNi_{5.0}$ amorphous films(ca. 1μm thick) were deposited on a polyimide membrane(Kapton, 40μm thick) at room temperature by means of the sputtering method. The $LaNi_{5.0}$ crystalline powder and pure Ni foil were used as reference materials. The procedure of activation to hydrogenate the sample was as follows. The samples prepared were transferred under an atmosphere of argon gas (99.999% Ar) into the stainless steel cell with X-ray transparent Kapton (75μm thick, Toray - du Pont Co., Ltd.) windows. A pressure of 1.0×10^6Pa of hydrogen (99.999%, H_2) was applied to the sample for 2 hours at 363K, then the cell was cooled to 273K in an ice-bath for 2 hours maintaining constant pressure. The heating-cooling process was repeated five times.

The procedure for the measurement of X-ray absorption spectra(XAS) were described in Chapter 1.

The XAS data of as-prepared samples were obtained in vacuo at 220K, and those of hydrogenated samples under constant pressures of 1.0×10^5 and 8.0×10^5 Pa at 220K using the cell mentioned above. The hydrogen content in $LaNi_5$ films was determined by a quartz-crystal mass-monitoring (QCMM) method.[9)]

The EXAFS data were analyzed in the same manner as described in Chapter 1.

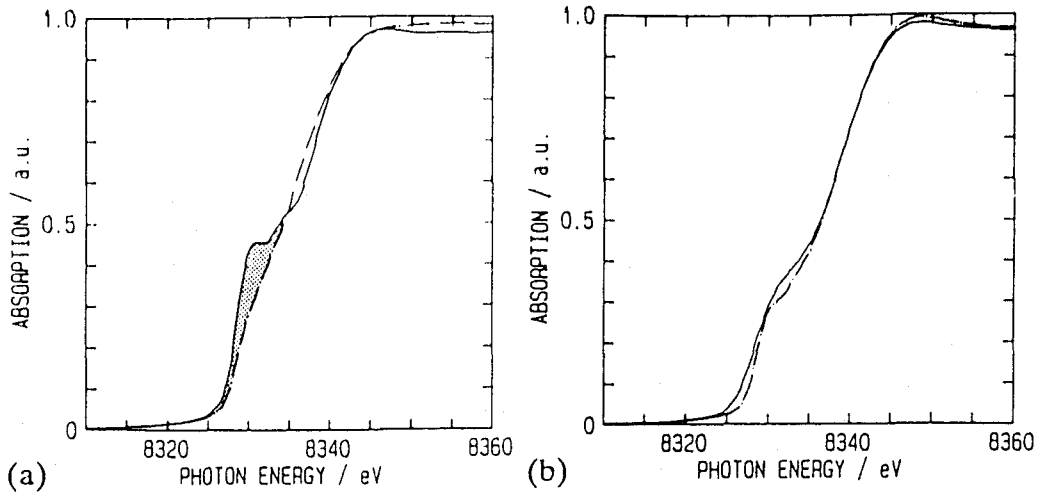

Fig. 2-1. Ni K-edge XANES spectra for $LaNi_5$ crystalline bulk(a) and amorphous film(b):
——— As-prepared
- - - - - - Hydrogenated(H_2 8.0×10^5 Pa)

2.3 Results and Discussion

Figure 2-1(a) shows Ni K-edge XANES spectra for $LaNi_{5.0}$ crystalline bulk and its hydride, $LaNi_{5.0}H_7$. The Ni K near-edge spectrum is associated with the $\ell = 1$(p-like) projected density of final states and the shape of the absorption edge reflects the extent of Ni 3d-4p hybridization. The difference in the spectra is the decrease in area at the edge (shaded area), resulting from less 3d-4p hybridization due to the narrowing of the Ni 3d-band. Calculation have shown that the Ni 3d-bands narrow from 3.2eV in $LaNi_5$ to less than 2.5eV in $LaNi_5H_7$ due in part to the large lattice expansion upon hydrogenation.[32] Garcia et al.[34] reported that in the $CeFe_2$ system, the Fe K-edge absorption peak at the absorption edge also decreased due to hydrogenation, and which can be

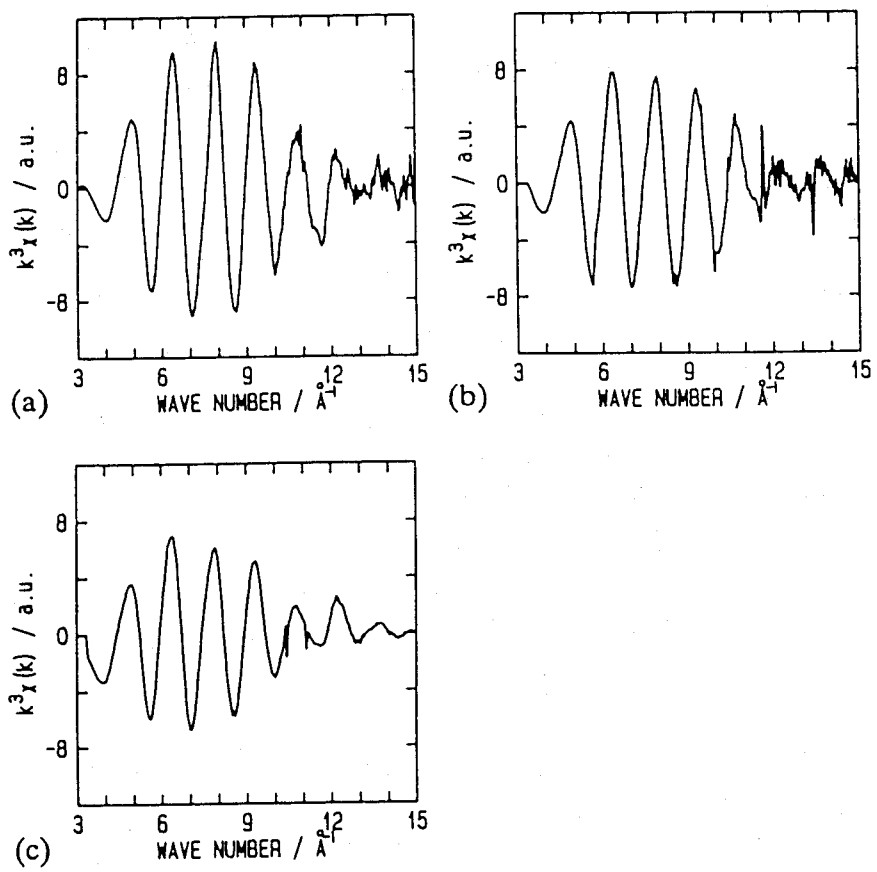

Fig. 2-2. Ni K-edge EXAFS in (a) the as-prepared film and its hydrides (b)$LaNi_{5.0}H_{1.0}$ and (c) $LaNi_{5.0}H_{1.2}$.

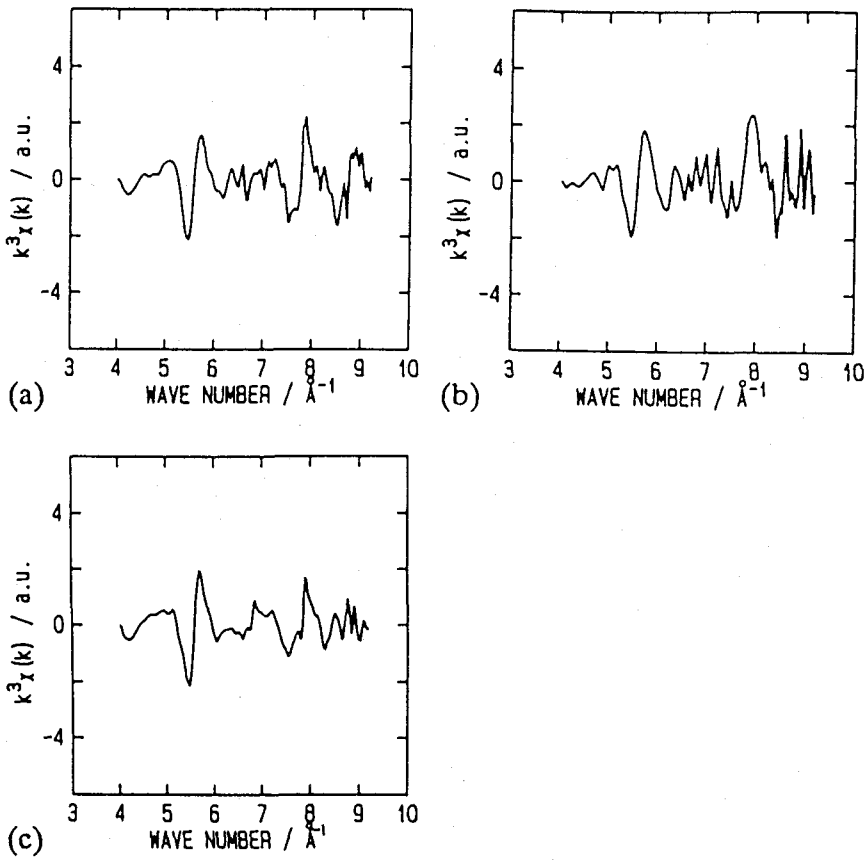

Fig. 2-3. La L_{III}-edge EXAFS in (a)the as-prepared film and its hydrides (b)$LaNi_{5.0}H_{1.0}$ and (c)$LaNi_{5.0}H_{1.2}$.

assigned to the decrease of p-d mixing and corresponding increased 3d electrons localization. Another possible interpretation obtained from the calculation for the difference in the line shapes at the edge is the modification of the nickel d-bands because of the formation of Ni-H bonding.

The shape of the absorption edge for the hydrogenated $LaNi_{5.0}$ amorphous film is almost the same as that for the as-prepared amorphous film as shown in Fig. 2-1(b). Therefore, it appears that hydrogen in amorphous film does not affect the width of the Ni 3d-band; i.e., the shape of the absorption edge, because a weakening 3d-4p hybridization had occurred at the amorphization of $LaNi_5$ as observed in Chapter 1.

Figures 2-2 and 2-3 show the k^3-weighted EXAFS spectra at Ni K- and La L_{III}-edges in the sputtered amorphous $LaNi_{5.0}$ films at various hydrogen contents.

Magnitudes of the Fourier transforms obtained by a Fourier analysis of the EXAFS data in these films are also shown in Figures 2-4 and 2-5. A large peak appeared on the Ni edge at about 2 Å corresponding to mainly Ni-Ni and partially Ni-La distances, while on the La edge at about 3 Å corresponding to the La-Ni distances. The profiles of the Fourier transforms in the hydrogenated samples show resemblance to those in the as-prepared ones, so that it was suggested that the local structures around central Ni and La atoms for the hydrogenated samples were

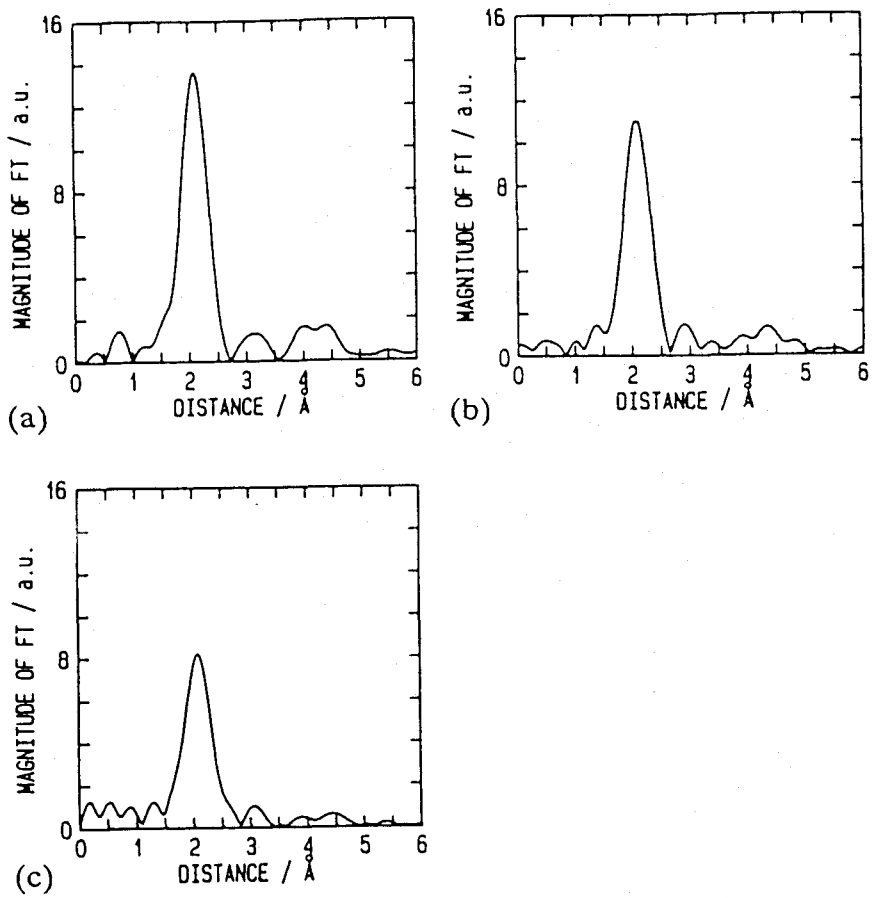

Fig. 2-4. Ni K-edge RSF in (a) the as-prepared film and its hydrides (b)$LaNi_{5.0}H_{1.0}$ and (c) $LaNi_{5.0}H_{1.2}$.

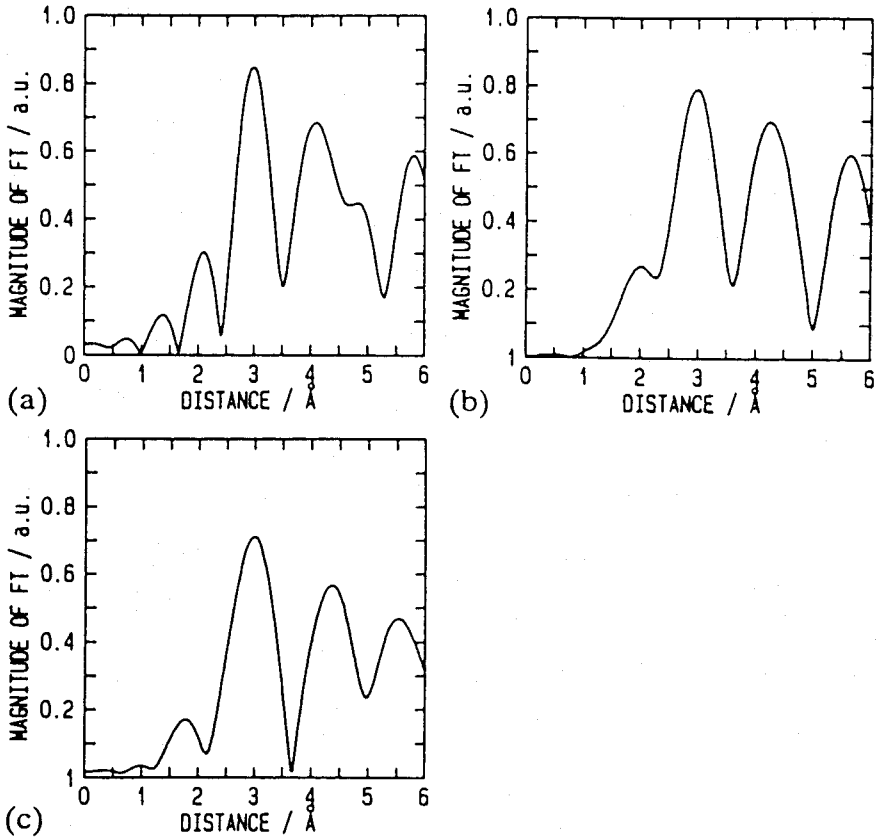

Fig. 2-5. La L_{III}-edge RSF in (a)the as-prepared film and its hydrides (b)$LaNi_{5.0}H_{1.0}$ and (c)$LaNi_{5.0}H_{1.2}$.

similar to those for the as-prepared ones. The main peak height of the Fourier transforms, however, decreases with increasing the hydrogen concentration. The damping of the main peak for the hydrogenated samples is assumed to occur by either decreasing the coordination number or increasing the static disorder induced by hydrogen.[28)]

The results of the curve fitting analysis on the Ni K- and La L_{III}- edges before and after hydrogenation are presented in Table 2-1(a) and (b). There are two kinds of Ni atoms having the different symmetry in $LaNi_5$ crystalline bulk, i.e. Ni_I atoms(coordination number:6) and Ni_{II} atoms(coordination number:4). From the previous chapter concerning EXAFS study of as-prepared $LaNi_{5.0}$ films, it has been revealed that the main peak in Ni RSF contains information on two subshells of Ni-Ni pairs (Ni_I-Ni_{II}, Ni_{II}-Ni_{II}) and one subshell of Ni-La (Ni_I-La) pair, whereas the peak in La RSF is related to two subshells of La-Ni pairs(La-Ni_I, La-Ni_{II}). These subshells were also adopted to analyze the after-hydrogenated samples.

The coordination number of each subshell for the as-prepared film was almost the same as that for the hydrogenated samples within the experimental error, and the interatomic distance of each subshell increased with the hydrogen concentration. Since the coordination number remained unchanged, the decrease of peak height observed for hydrogenated films compared with as-prepared films, as shown in Figures 2-4 and 2-5 is due solely to an

Table 2-1. Structural parameters at the Ni K-edge (a) and the La L_{III}-edge (b) for the $LaNi_{5.0}$ amorphous film and its hydrides.

(a)

N	L(Å)	σ^2 (Å$^2\times10^{-3}$)	R
As-prepared film			
4.6Ni ± 0.5	2.46 ± 0.01	6.8	
3.5Ni ± 0.9	2.57 ± 0.02	13.2	4.8×10^{-3}
1.7La ± 1.4	2.92 ± 0.08	14.6	
Hydrogenated film ($LaNi_{5.0}H_{1.0}$)			
4.6Ni ± 0.6	2.47 ± 0.01	7.6	
3.5Ni ± 1.2	2.60 ± 0.02	14.3	7.2×10^{-3}
1.7La ± 1.7	2.94 ± 0.10	15.9	
Hydrogenated film ($LaNi_{5.0}H_{1.2}$)			
4.6Ni ± 0.5	2.47 ± 0.01	8.6	
3.6Ni ± 0.9	2.61 ± 0.02	13.2	5.4×10^{-3}
1.8La ± 1.4	2.95 ± 0.08	17.5	

N real coordination number ; L interatomic distance; σ Debye–Waller factor; $R=(\{\Sigma_k[\chi_{obs}(k)-\chi_{calc}(k)]^2\}/[\Sigma_k\chi_{obs}(k)]^2)^{1/2}$.

(b)

B	L (Å)	σ^2 (Å$^2\times10^{-2}$)	R
As-prepared film			
1.3Ni ± 0.1	3.01 ± 0.01	2.1	
2.8Ni ± 0.2	3.27 ± 0.01	2.1	6.6×10^{-3}
Hydrogenated film ($LaNi_{5.0}H_{1.0}$)			
1.5Ni ± 0.2	3.03 ± 0.02	2.4	
2.7Ni ± 0.3	3.31 ± 0.02	2.0	5.7×10^{-3}
Hydrogenated film ($LaNi_{5.0}H_{1.2}$)			
1.6Ni ± 0.2	3.05 ± 0.02	2.5	
2.8Ni ± 0.2	3.30 ± 0.02	2.2	5.4×10^{-3}

B apparent coordination number; L interatomic distance; σ Debye–Waller factor; $R=(\{\Sigma_k[\chi_{obs}(k)-\chi_{calc}(k)]^2\}/[\Sigma_k\chi_{obs}(k)]^2)^{1/2}$.

increase in the Debye-Waller factor. The EXAFS study on hydrogenation of palladium clusters supported on alumina showed that the increase in the Debye-Waller factor for the hydrogenated sample indicates the structural disorder due to the interstitial hydrogen.[35)]

It is well known that an interatomic distance in the $LaNi_5$ crystalline bulk increases owing to the phase transformation from the α to β-phase. This generates microcracks, and then pulverization of the alloy occurs. The crystal structure of the α-phase has been studied by Soubeyroux et al.[13)] and that of the β-phase by Lartigue et al.[10,12)] by means of powder neutron diffraction. Figure 2-6 illustrates the dependence of hydrogen concentration on the interatomic distance in the amorphous film and the crystal- line bulk using an example of Ni_I-Ni_{II} pair. On the crystalline bulk, the β-phase appears at about $0.4H/LaNi_5$. Subsequently, the sudden increase in Ni_I-Ni_{II} distance is observed at the hydrogen concentration.[13)] The increase in Ni_I-Ni_{II} interatomic distance with hydrogen concentration for the amorphous film was in agreement with that for the α-phase in the crystalline bulk, and the tendency was maintained up to $1.2H/LaNi_5$. This appears to be one of the reasons for which amorphous films do not pulverize.

The differences in the mechanism of phase transformation between the amorphous film and the crystalline bulk can be attributed to the differences in the process of occupation of

hydrogen sites. EXAFS analyses have shown the similarity of the short range order between the amorphous film and the crystalline bulk. Therefore, the hydrogen sites having the same structure as D1, D3 and D5 sites in the crystalline bulk proposed by Lartigue et al.[12] appear to exist also in the amorphous film.

Absorbing hydrogen, the crystalline bulk forms an α-phase where a part of D5 sites are occupied with hydrogen up to $0.4H/LaNi_5$, and a β-phase is formed with large lattice expansion when more hydrogen atoms enter a part of D1 or D3 sites, especially D1 sites are occupied causing a displacement of the Ni_I atoms in the c-direction and a further increase in the Ni_I-Ni_{II} interatomic distances.[11] In the case of the amorphous film, a part of D5 sites may be occupied with hydrogen up to $1.2H/LaNi_5$, whereas D1 and D3 sites remain unoccupied, so that the increase in

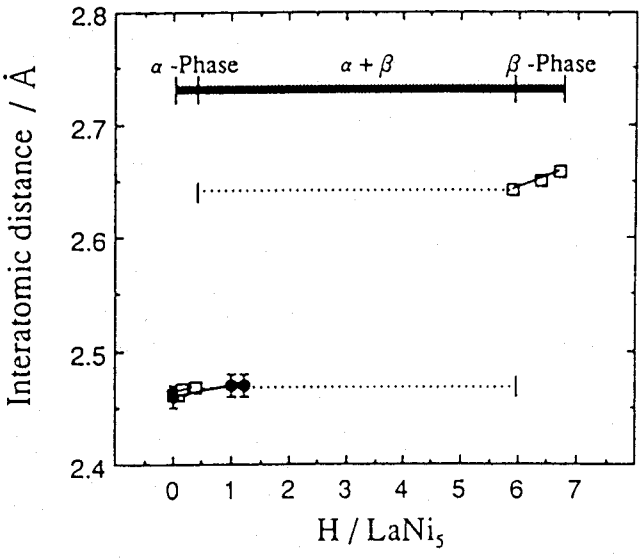

Fig. 2-6. Hydrogen concentration dependance of the Ni_I-Ni_{II} interatomic distance: □, crystalline bulk; ● , amorphous film.

Ni_I-Ni_{II} interatomic distance appears to be relatively small. For the above reasons, amorphous films exhibited excellent durability to the hydrogen absorption-desorption cycling process in comparison with the crystalline bulk.

The significant difference in the interatomic distance and Debye-Waller factors were observed between the amorphous film and crystalline bulk at both the Ni-K and La-L_{III} edges. The Debye-Waller factors express variations from the average interatomic distances. These differences cause the differences in the size of the hydrogen sites and variations in the amount of hydrogen taken up by the alloys.

In order to clarify the relationship between the structural parameters and the size of the hydrogen sites, we expressed the size of the site using the radius of a sphere inscribed in the metal atoms which make up the site. Radii of the metal atom were used as metallic bond radii(r_{La}=1.88 Å, r_{Ni}=1.25 Å).[11] In other words, the difference in the size of the hydrogen sites is reflected by the difference in the inscribed spherical radius. This inscribed spherical radius is derived by taking the interatomic distances and the Debye-Waller factors obtained from the EXAFS analysis to the distances of the atom-atom pairs that comprise the hydrogen site.

In order to show the degree of variation for the inscribed spherical radius at the hydrogen site, it is necessary to substitute the average interatomic distance and the standard deviation for the

resultant inscribed spherical radius and their standard deviation.

To determine the average radius, r_0, and the standard deviation, d, of the inscribed sphere, we took the distances $L+\sigma$ and $L-\sigma$ that derived from the Debye-Waller factor, σ^2, and the interatomic distance, L.

Then the Gaussian distribution function, g(r), for the inscribed spherical radius was obtained as the following equation:

$$g(r) = \frac{1}{\sqrt{2\pi}d} \exp\{-(r-r_0)^2/2d^2\}$$

The D1 and D3 sites are a tetrahedral sites consisted of four metal atoms. The inscribed sphere of these sites inscribe all these four atoms. As for the D5 site, the site is an octahedral site surrounded by two $N1_I$, two Ni_{II} and two La atoms, but hydrogen is not found in the center of this octahedral site. Instead, we find

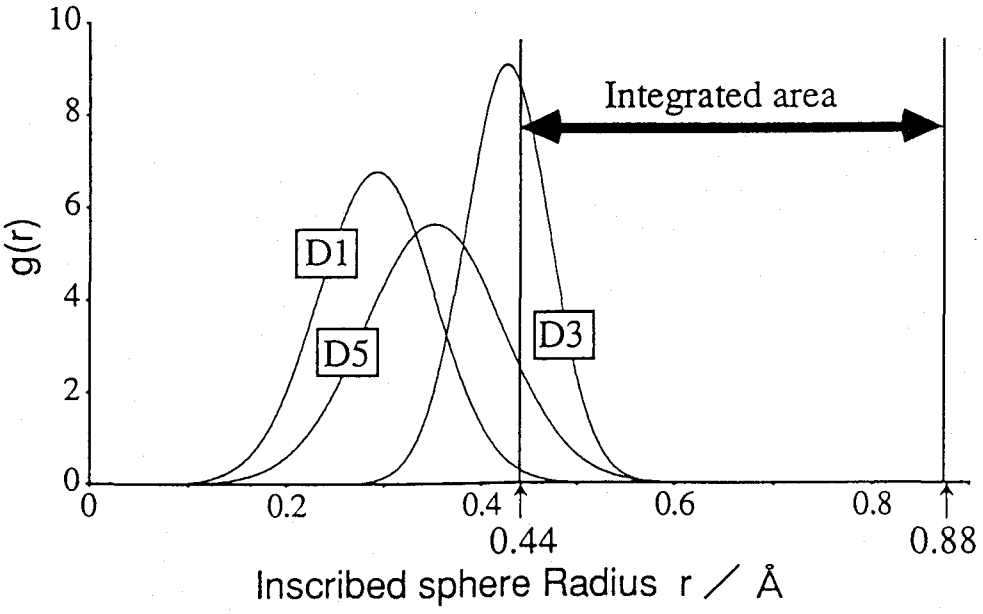

Fig. 2-7. Distribution of the size of each hydrogen site for the amorphous $LaNi_{5.0}$ alloy.

Table 2-2. Estimation of the number of hydrogen atoms in the sites for amorphous $LaNi_{5.0}$ films.

	Crystalline bulk	Amorphous alloy
D1	1	0.01
D3	3	1.15
D5	3	0.31
Total H/$LaNi_5$	7	1.47

the hydrogen in a tetrahedral site surrounded by the single Ni_{II}, single La and two Ni_I atoms that comprise the site.

The standard deviation and the average inscribed spherical radius for the D1, D3 and D5 sites in the amorphous film can be obtained, and the respective Gaussian distribution functions are provided in Fig. 2-7.

The lower limit for the radius of the inscribed sphere where hydrogen can exist is known to be 0.44 Å,[36] and since we know that two hydrogen atoms cannot occupy a site, the upper limit was set at 0.88 Å. If we integrate the Gaussian distribution function given in Fig. 2-7 within this range, then we get a rate of hydrogen occupancy for the D1, D3 and D5 sites in the amorphous films. If we focus on the rate of hydrogen occupancy for the D1, D3 and D5 sites in the amorphous film, the rate of hydrogen occupancy (38.3%) at the D3 site is found to be relatively larger than that at

the D1 and D5 sites. This is a good indication that differences in the rate of hydrogen occupancy at the D3 site largely affect differences in the hydrogen concentration.

By multiplying the rate of hydrogen occupancy obtained for each D1, D3 and D5 site in the amorphous films as shown in Table 2-2 by the number of hydrogen atoms (1 at the D1 site, 3 at the D3 site, and 3 at the D5 site) at each hydrogen site per crystalline bulk formula weight, then we get the number of hydrogen atoms at each site. The sum of the number of hydrogen atoms at each site gives the hydrogen concentration, $H/LaNi_{5.0} = 1.47$, for the amorphous film, and this tendency to decrease in hydrogen concentration for the amorphous film in comparison with the crystalline bulk, $H/LaNi_{5.0} \fallingdotseq 6$, is consistent with that from the experimental result that the maximum hydrogen concentration, $H/LaNi_{5.0} = 1.9$, for the amorphous film is smaller than that for the crystalline bulk.

2.4 Conclusion

The local structures around La and Ni atoms in amorphous $LaNi_5$ films and their hydrides have been clarified with EXAFS.

It was revealed that the decrease in the hydrogen concentration for the amorphous film as compared to the crystalline bulk can be estimated by the calculation on the basis that the hydrogen prefers to occupy the sites with optimum size.

The hydrogen-induced increase in the distance of the Ni_I-Ni_{II} pairs for the amorphous film was found to be consistent with that for the α-phase in the crystalline bulk, and this appears to prevent the amorphous films from pulverizing.

Chapter 3

The Local Structures of an Amorphous $LaNi_{5.0}$ Alloy Having the Large Hydrogen Density

3.1 Introduction

The hydrogen density which is an important property for application is, however, much smaller for the amorphous films than for the crystalline bulk.[19)]

Recently, the capability of hydrogen absorption for an amorphous $LaNi_{5.0}$ film prepared by reactive sputtering was found to be superior to that by conventional sputtering as shown in Fig. 3-1.[37)]

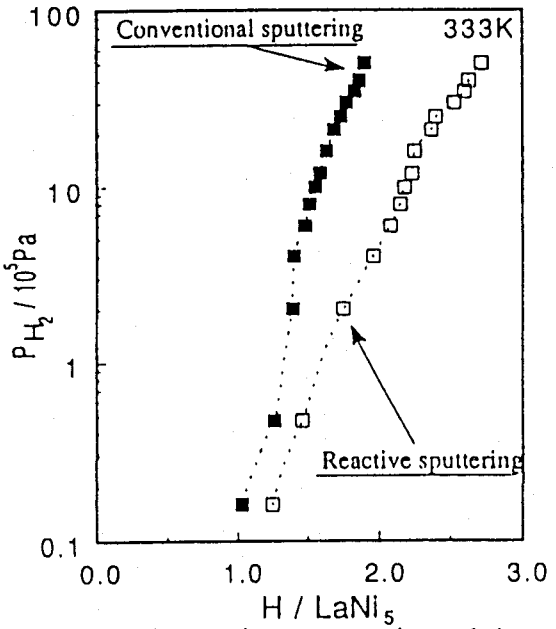

Fig. 3-1. Hydrogen absorption properties of the conventional and the reactive sputtered films.

In this chapter, we investigated the local structure of amorphous $LaNi_{5.0}$ films by using EXAFS and focused on the question whether there exists an influence on the atomic arrangement of the production method, namely reactive and conventional sputtering.

3.2 Experimental

Films of amorphous $LaNi_{5.0}$ having a thickness of 1μm were deposited by a rf magnetron sputtering apparatus on a 40μm thick Kapton membrane. For a reactive sputtering, an Ar(50mol%)-H_2(50mol%) gas mixture was used as a sputtering gas and a pressure of the gas was 0.66Pa. The film deposition rate was 2.8nm•s^{-1} at the 400W rf input power. On the other hand, a sputtering gas for a conventional sputtering was 99.9999% pure Argon and the resulting deposition rate was 6.0nm•s^{-1}.

For the preparation of hydrogenated films, the hydrogen gas was applied to the as-prepared films mounted in the stainless-steel cell with a Kapton window. The hydrogen content in the films was estimated by a quartz-crystal mass-monitoring method.

The XAS data were collected at 220K under vacuum for the as-prepared films while under hydrogen atmospheres of 1.0×10^5 and 8.0×10^5Pa for the hydrogenated films.

Typical Fourier filtering parameters were: K weight=3, K range=4.0-9.2Å^{-1} (La edge), 3.3-14.0Å^{-1}(Ni edge) and R

range=2.4-3.4Å(La edge),1.6-2.7Å(Ni edge).

3.3 Results and Discussion

EXAFS spectra and their radial structure function (RSF) for amorphous $LaNi_{5.0}$ films prepared by reactive (RS-film) or conventional (CS-film) sputtering are shown in Fig.3-2.

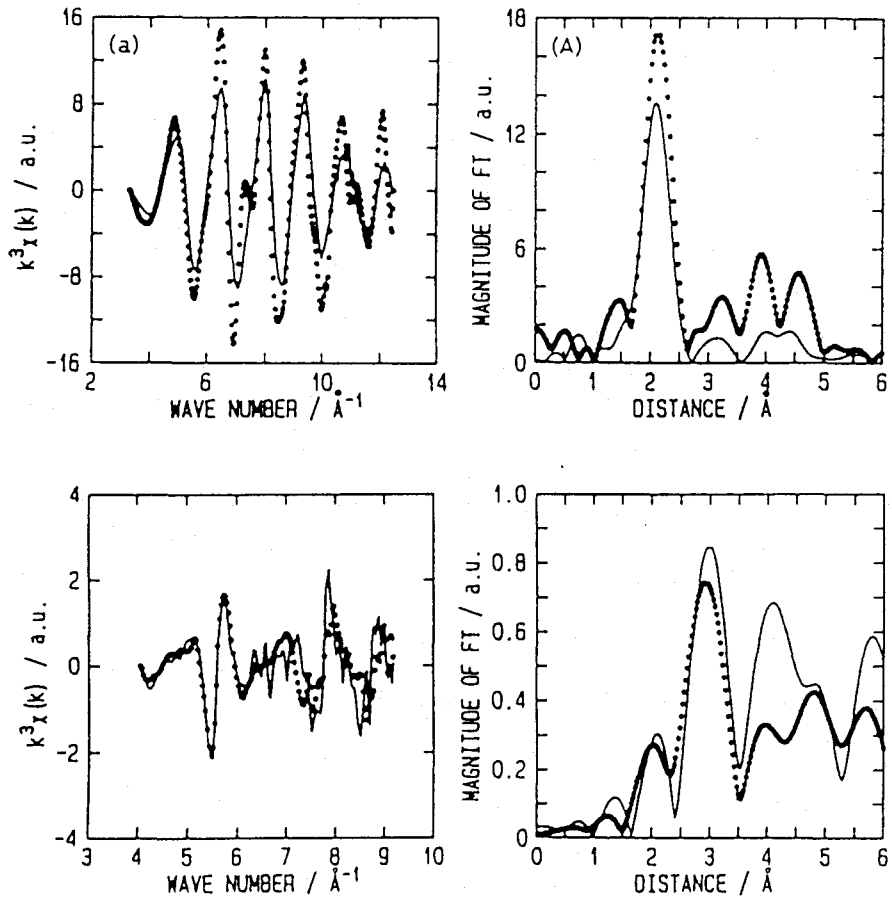

Fig. 3-2 EXAFS Spectra (a, b) and magnitudes of Fourier transforms (A, B) in amorphous $LaNi_{5.0}$ films. (a, A) : Ni K-edge, (b, B) : La L_{III}-edge

····· Reactive sputtered film

——— Conventional sputtered film

The local structure of both films appears to be independent of the method of film preparation because of the similar peak profile on the RSF. At the Ni K-edge, however, the magnitude of the main peak was larger for the RS-film than for the CS-film. On the other hand, at the La L_{III}-edge, the opposite relationship was observed.

The results of the curve fitting analyses are presented in Table 3-1. The coordination numbers and the interatomic distances of the RS-film coincided with those of the CS-film within errors, so that both films appear to resemble each other in the local structure. It is noteworthy that the Debye-Waller factors at the Ni edge were obviously smaller for the RS-film than for the CS-film, while those at the La edge were smaller for the CS-film than for the RS-film. It was suggested that we cannot study the correlation between the hydrogen absorption characteristics and the structural parameters obtained from the analyses of each absorption edge, but we must combine the information obtained from both edges.

According to the procedure as described in Chapter 2, the hole radius of interstitial sites accommodated with hydrogen in the $LaNi_{5.0}$ films were calculated using the interatomic distances and the Debye-Waller factors obtained from EXAFS analyses (Table 3-2). It was stipulated that the hydrogen sites of both the RS-film and the CS-film are the same as those of the crystalline bulk, because there was no remarkable difference of short range order between

Table 3-1. Structural parameters at the Ni K-edge and the La-L_{III} edge for amorphous $LaNi_{5.0}$ films.

Centrtal atom	Reactive sputtered film N	L(Å)	σ^2(Å$^2\times10^{-3}$)	R	Conventional sputtered film N	L(Å)	σ^2(Å$^2\times10^{-3}$)	R
Ni	4.5±0.5Ni	2.47±0.01	5.0		4.6±0.5Ni	2.46±0.01	6.8	
	3.5±0.7Ni	2.58±0.01	7.7	4.9×10^{-3}	3.5±0.9Ni	2.57±0.02	13.2	4.8×10^{-3}
	1.7±1.4La	2.90±0.06	11.2		1.7±1.4La	2.92±0.08	14.6	
Centrtal atom	Reactive sputtered film B	L(Å)	σ^2(Å$^2\times10^{-3}$)	R	Conventional sputtered film B	L(Å)	σ^2(Å$^2\times10^{-3}$)	R
La	1.3±0.5Ni	3.01±0.01	2.8		1.3±0.1Ni	3.01±0.01	2.1	
	2.8±0.3Ni	3.30±0.01	2.5	10.5×10^{-3}	2.8±0.2Ni	3.27±0.01	2.1	6.6×10^{-3}

L, interatomic distance; N, real coordination number; B, apparent coordination number;
σ, Debye-Waller factor; $R=[\{\Sigma_k(\chi_{obs}(k)-\chi_{calc}(k))^2\}/\{\Sigma_k\chi_{obs}(k)\}^2]^{1/2}$

Table 3-2. Description of interstitial sites in amorphous $LaNi_{5.0}$ films.

Site[a]	Coordination	Hole radius(Å)[b]			
		RS-film		CS-film	
		ave.	σ	ave.	σ
D1	1NiII+3NiIII	0.298	0.050	0.292	0.059
D3	2La+2NiII	0.439	0.056	0.427	0.044
D5	1La+2NiII+1NiIII	0.347	0.073	0.351	0.071

[a]The hydrogen sites exist in the $LaNi_5$ crystalline bulk.
[b]The largest interstitial spherical hole. The radii of the hole of each site were calculated by the close-packed model.

the amorphous films and the crystalline bulk except for the Debye - Waller factors.

Table 3-3 shows the number of hydrogen atoms which occupy each site in the amorphous films. It was revealed that the total number of hydrogen atoms was larger for the RS-film(1.79) than for the CS-film(1.47). This is because the fluctuation of static disorder for the atoms which constitute the hydrogen sites is smaller for the RS-film than for the CS-film, so that the rate of occupancy for the D3 site increases. It was reported that the hydrogen density of the RS-film is one and a half times larger than that of the CS-film.[37] Consequently, the largeness of hydrogen density observed for the RS-film appears to be due to the increase in the rate of occupancy for the D3 site caused by the small structural fluctuation.

Table 3-3. Estimation of the number of hydrogen atoms in the sites for amorphous $LaNi_{5.0}$ films.

Site	Ratio of occupancy(%)*			Number of atoms occupied		
	Bulk	RS-film	CS-film	Bulk	RS-film	CS-film
D1	100	0.207	0.608	1	0.00207	0.00608
D3	100	49.3	38.3	3	1.48	1.15
D5	100	10.1	10.4	3	0.312	0.312
			Total	7	1.79	1.47

*A minimum hole size to accept hydrogen of 0.44 Å was adoptted to be the estimation.

3.4 Conclusion

In order to clarify the reason why the hydrogen density of the RS-film is larger than that of the CS-film, the local structure in the films was investigated using EXAFS. Although the coordination numbers and the interatomic distances of both films coincided each other, the Debye-Waller factors were found to be smaller for the RS-film than for the CS-film, indicating the RS-film has the small structural fluctuation compared with the CS-film.

The rate of occupancy of hydrogen atoms for the D3 site, which is calculated by considering the Debye-Waller factors, was larger for the RS-film than for the CS-film.

Chapter 4

Comparison of the Local Structure of the Amorphous $LaNi_{5.0}$ Alloys Prepared by Evaporation and Sputtering

4.1 Introduction

Amorphous $LaNi_{5.0}$ films have been succeeded in obtaining by two different methods, namely flash evaporation[18] and sputtering. The EXAFS studies on the amorphous $LaNi_{5.0}$ sputtered films and their hydrides have been performed in Chapter 1-3.

In this chapter, we have studied the local structure around La and Ni atoms of amorphous evaporated films and investigated the difference of the local structure between in the amorphous evaporated and sputtered films, furthermore, the change in the local structure due to absorption of hydrogen by using EXAFS.

4.2 Experimental

Lanthanum-nickel alloys used were supplied by Santoku Metal Industry, Kobe. The $LaNi_{5.0}$ evaporated films of about 1μm thick were prepared by a flash evaporating method onto a polyimide

membrane(Kapton, 40μm thick, Toray-du Pont Co. Ltd.). La-Ni alloy powder mixture consisted of $LaNi_{5.0}$(98 wt%) and $LaNi_{3.0}$(2 wt%) was fed to a preheated tungsten boat(2.3×10^3K) by a conveyor belt furnished with a hopper and was evaporated immediately. The procedure of preparation and characterization of $LaNi_{5.0}$ sputtered amorphous films was described in Chapter 1.

To obtain a clear jump at the absorption edge, we stacked the $LaNi_{5.0}$ films and the total thickness of the films used for the XAS measurements were about 35 and 20μm for the La and Ni edges respectively. The XAS data of as-prepared samples were collected under vacuum at 220K. As for the hydrogenated samples, we measured the XAS under atmosphere of hydrogen at constant pressures of $1.0\text{x}10^5$ and $8.0\text{x}10^5$Pa using the cell mentioned above.

4.3 Results and Discussion

Fig. 4-1 (a) and 1(b) show the k^3-weighted EXAFS and its RSF at Ni K-edge for the amorphous $LaNi_{5.0}$ evaporated film in comparison with those for the sputtered film. The EXAFS oscillations and the profiles of RSF for both evaporated and sputtered films well coincided each other. RSF at Ni K-edge and La L_{III}-edges for the evaporated film(a) and its hydride(b) are shown in Figs. 4-2 and 4-3. The profiles of the RSF for the

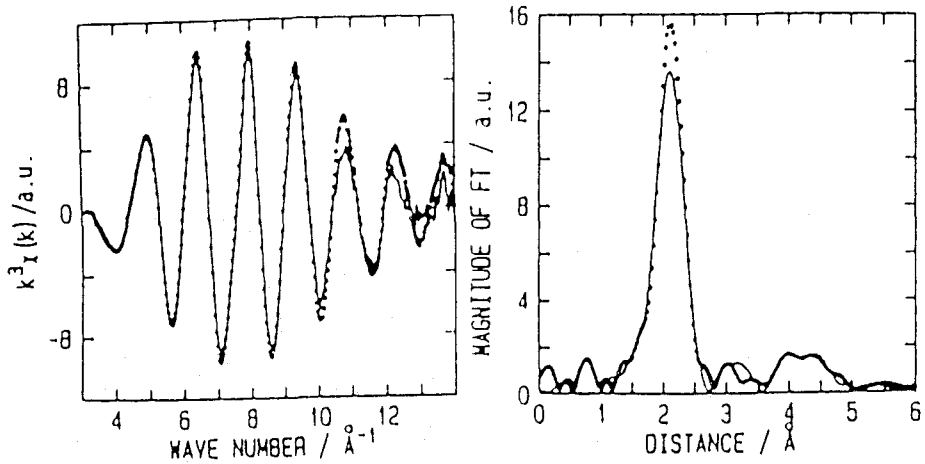

Fig. 4-1. Ni K-edge EXAFS(a) and RSF(b) spectra for amorphous $LaNi_{5.0}$ films.
···· Evaporated film, — Sputtered film

hydride resemble those for the as-prepared ones, so that the local structures around central Ni and La atoms in the hydrides appears to be similar to those in the as-prepared ones. The damping of the main peaks for the hydrides compared with the as-prepared films indicate the structural disorder due to the interstitial hydrogen.[35)]

In $LaNi_{5.0}$ crystalline bulk, Ni atoms are classified into two different groups(Ni_I and Ni_{II}) having the different symmetry. In our previous EXAFS study of the sputtered amorphous $LaNi_{5.0}$ films, it has been revealed that main peak appeared on the Ni K-edge RSF at about 2 Å contained information on two subshells of Ni-Ni pairs(Ni_I-Ni_{II}, Ni_{II}-Ni_{II}) and one subshell of Ni-La pair(Ni_I-La) whereas on the La L_{III}-edge RSF about 3 Å related to two subshells of La-Ni pair(La-Ni_I, La-Ni_{II}). Therefore, we also adopted these subshells to analyze the evaporated films and their hydrides.

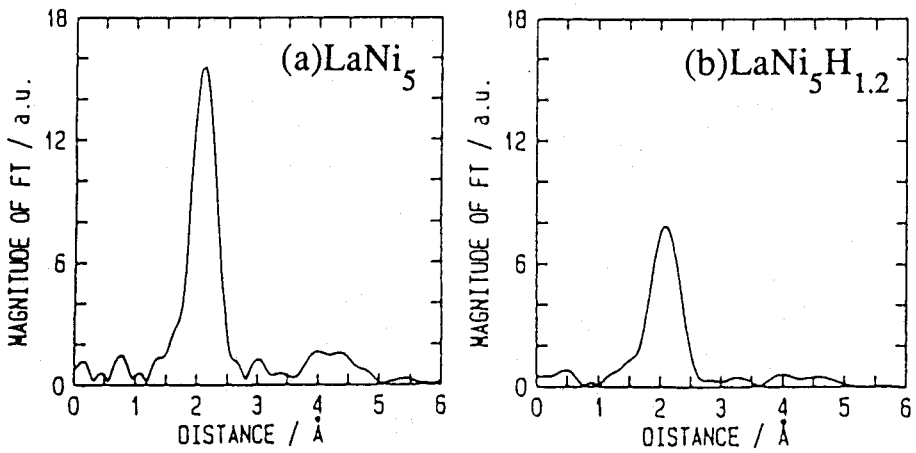

Fig.4-2. Ni K-edge RSF spectra for the evaporated $LaNi_{5.0}$ film(a) and its hydride(b).

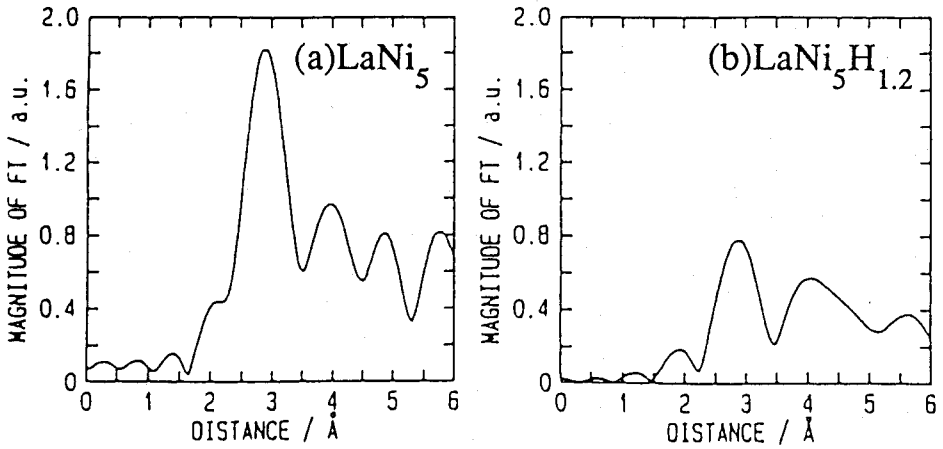

Fig. 4-3. La L_{III}-edge RSF spectra for the evaporated $LaNi_{5.0}$ film(a) and its hydride(b).

Table 4-1. Structural parameters for $LaNi_{5.0}$ films as prepared by evaporating and sputtering.

Centrtal atom	Evaporated film N	L(Å)	σ^2(Å$^2\times10^{-3}$)	R	Sputtered film N	L(Å)	σ^2(Å$^2\times10^{-3}$)	R
Ni	4.5±0.3Ni	2.46±0.01	5.8		4.6±0.5Ni	2.46±0.01	6.8	
	3.4±0.9Ni	2.59±0.01	13.5	2.1×10^{-3}	3.5±0.9Ni	2.57±0.02	13.2	4.8×10^{-3}
	1.7±1.4La	2.93±0.06	16.6		1.7±1.4La	2.92±0.08	14.6	
Centrtal atom	Evaporated film B	L(Å)	σ^2(Å$^2\times10^{-3}$)	R	Sputtered film B	L(Å)	σ^2(Å$^2\times10^{-3}$)	R
La	1.5±0.3Ni	3.02±0.02	2.2		1.3±0.1Ni	3.01±0.01	2.1	
	2.8±0.3Ni	3.30±0.01	1.5	6.2×10^{-3}	2.8±0.2Ni	3.27±0.01	2.1	6.6×10^{-3}

L, interatomic distance; N, real coordination number; B, apparent coordination number;
σ, Debye-Waller factor; $R=[\{\Sigma_k(\chi_{obs}(k)-\chi_{calc}(k))^2\}/\{\Sigma_k\chi_{obs}(k)\}^2]^{1/2}$

The results of the curve fitting analysis on the Ni and La edges are presented in Table 4-1. Judging from the error, the interatomic distance of the third subshell(Ni_I-La) at the Ni edge is unreliable, so that the Ni_I-La distance measured from the Ni edge appears to be inconsistent with that from the La edge. The coordination number at the La edge is an apparent coordination number, B(=N×S; N, real coordination number, S, damping factor). There is no adequate reference material to determine the S value for the La edge, so that N at the La edge is not obtained at the present stage.

The structural parameters for the as-prepared evaporated film agree with those for the sputtered film. Therefore, it was suggested that the short range order in the evaporated film resembles that in

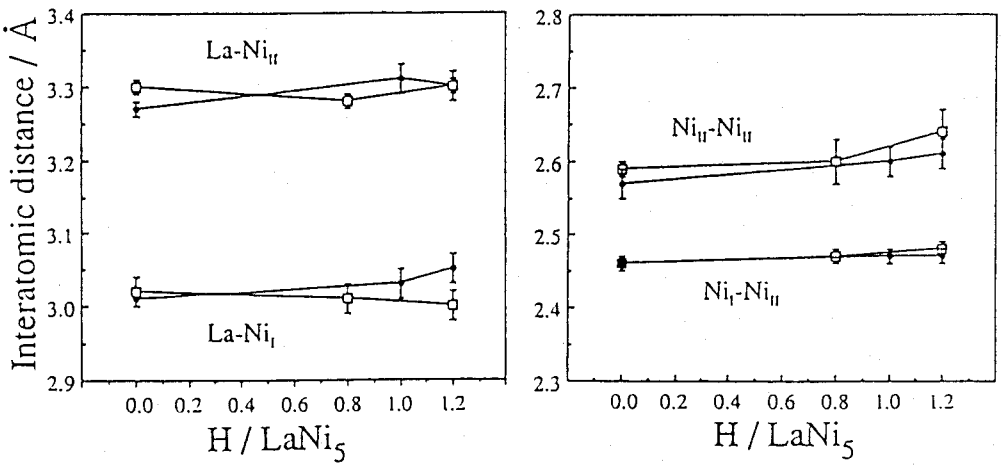

Fig. 4-4. Variation of interatomic distances as a function of the hydrogen content.

□ ···· Evaporated film

● ····Sputtered film

the sputtered film.

Fig. 4-4 illustrates the dependence of hydrogen concentration on the interatomic distances in the evaporated film and the sputtered film. The change in the interatomic distances with hydrogen density for the evaporated film was in agreement with that for the sputtered film. The coordination number of each subshell for the evaporated film was almost the same as that for the sputtered films within the experimental error.

From the knowledge obtained from Chapter 1., it has become apparent that the short range order in the sputtered amorphous film were similar to that in the crystalline bulk, so that hydrogen atoms in the sputtered film appeared to be accommodated in the interstitial sites having the same structure as D_1, D_3 and D_5 hydrogen sites in the crystalline bulk. Therefore, the hydrogen sites in the sputtered film appear to exist also in the evaporated film.

4.4 Conclusion

We have compared the local structure around La and Ni atoms between the evaporated and sputtered $LaNi_{5.0}$ films. The local structure in the as-prepared evaporated film was similar to that in the sputtered one, and the change in the local structure in the evaporated film with increasing hydrogen concentration also resembled that in the sputtered one. This indicates that the

hydrogen sites in the evaporated film are similar to those in the sputtered one.

Chapter 5

Correlation between the Local Structures and the Electronic States of $LaNi_5$ Alloy hydrides

5.1 Introduction

As described in Chapter 1-4., the hydrogen occupation into the interstitial sites of metal host framework in both the amorphous and crystalline state appears to depend on the configuration of metal atoms surrounding hydrogen atoms. Ultimately, the stability of hydrogen in the metal-hydrogen system appears to originate from the electronic states of a small local region of the system involving the hydrogen atom and its surrounding metals.

In the first place, it is necessary to clarify whether the electronic state of local region of the $LaNi_5$ alloy hydride system is related to the hydrogen absorption properties of these system or not.

The electronic states of β-phase $LaNi_5$ alloy hydride, $LaNi_5H_7$, was previously calculated using tight-binding approximation method,[32] and this is the only example of electronic structure calculation treating the $LaNi_5$ alloy hydride. This method uses an orthogonal basis set, in other words, the overlap integral between near neighbor atomic orbitals is regarded

as nil, so that the bonding state between atoms of some interest appears to be unable to evaluate.

When the $LaNi_5$ alloy is hydrogenated at room temperature, it forms a phase called the α-phase where up to 0.4H can be accommodated per formula unit.[38] The crystal structure of these phases has rarely been studied, since it is difficult to prepare crystals of these phases with weak hydrogen concentration.

The positions of hydrogen sites in the α-phase $LaNi_5$ hydride, namely, $LaNi_5D_{0.1}$ and $LaNi_5D_{0.4}$, have been investigated by Soubeyroux et al.[13] using a powder neutron diffraction technique and 3f, 6m and 12n sites in the P6/mmm space group were found to be occupied. On the other hand, Hempelman et al.[15] clarified the occupation of hydrogen in 3f and 6m sites in $LaNi_5H_{0.15}$ as a result of inelastic neutron scattering experiments and also elucidated the hydrogen occupation of the 3f site is about three times greater than that of the 6m site. Owing to the lack of accuracy in the determination of the hydrogen positions of such weak hydrogen systems, it is difficult to determine the hydrogen sites accurately from the experimental result alone.

In this chapter, the author present the calculation results of electronic states for the 3f and 6m site model clusters with or without hydrogen and reveal the reason for the origination of selective hydrogen occupation into these two sites.

Absorbing hydrogen, the $LaNi_5$ alloy forms the α-phase where a portion of the 3f and/or 6m sites are occupied by

hydrogen up to 0.4H/$LaNi_5$. The three 3f sites and six 6m sites exist in an unit cell, so that 0.4H/$LaNi_5$ means that there are many unit cells with no hydrogen. Thus, in the α-phase $LaNi_5$ hydride, the periodicity of the $LaNi_5$ crystal is lost and the band structure calculation method using a periodic potential of the $LaNi_5$ crystal is no longer usable. In order to calculate the electronic states of the α-phase $LaNi_5$ hydrides in which the periodicity of the $LaNi_5$ crystal is lost, we clarified the electronic states of a model cluster representing the α-phase $LaNi_5$ hydrides using a discrete variational (DV) Hartree-Fock-Slater Xα method that is a molecular orbital (MO) computing method,[17,39] and evaluated the interatomic bonding states using Mulliken's population analysis.[40,41]

There has been an attempt to calculate the local electronic state applying an ab-initio method by thinking of cluster models as reflecting part of the bulk of simple metal-hydrogen systems. Adachi et al.[42,43] have shown that the electronic states of the model cluster of transition metal hydrides is closely related to the heat of hydride formation.

5.2 Calculation

The crystal structure of a $LaNi_5$ alloy is a hexagonal $CaCu_5$ type in the P6/mmm space group. The unit cell with the lattice parameters a=5.01 Å and c=3.98 Å contains one La, two Ni_I and three Ni_{II} atoms. Ni atoms are classified into Ni_I and Ni_{II} with

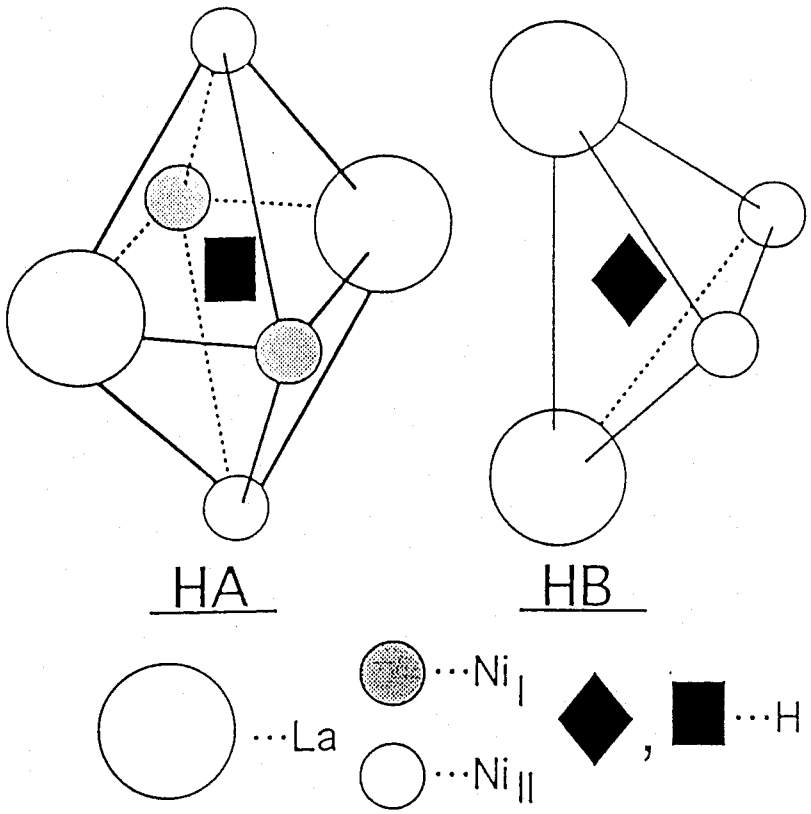

Fig. 5-1. Model clusters used in the calculations of α-$LaNi_5$ alloy hydrides.

different coordination environments.[32]

When hydrogen is absorbed by a $LaNi_5$ alloy under a hydrogen pressure of 2.23×10^5 Pa at 298 K, the α-phase hydride, $LaNi_5H_{0.1}$, was formed with a slight lengthening of lattice parameters(a=5.02 Å, c=3.98 Å).[13]

The model clusters HA and HB (Fig. 5-1) represent the two hydrogen sites, 3f and 6m respectively, in the α-phase $LaNi_5$ alloy. As model clusters of the $LaNi_5$ alloy before hydrogen absorption, we took clusters A and B, i.e., HA and HB clusters from which hydrogen had been removed. The atomic positions and interatomic distances of these clusters were determined based on the lattice parameters of corresponding bulk materials.

The LCAO numerical basis sets used in the calculation were 1s, 2s, 2p, 3s, 3p, 3d , 4s and 4p for a Ni atom , 1s, 2s, 2p, 3s, 3p, 3d , 4s, 4p, 4d, 4f, 5s, 5p, 5d, 6s and 6p for a La atom and 1s for a H atom. The potential in the cluster is derived from superposing the charges and static potentials of constituent atoms.

5.3 Results and discussion

We can obtain a density of states (DOS) curve by replacing each molecular orbital energy levels at ε_l with a Lorentzian, $n_l(\varepsilon)$, expressed as

$$n_l(\varepsilon)=f_l\sigma/\pi\{(\varepsilon-\varepsilon_l)^2+\sigma^2\}$$

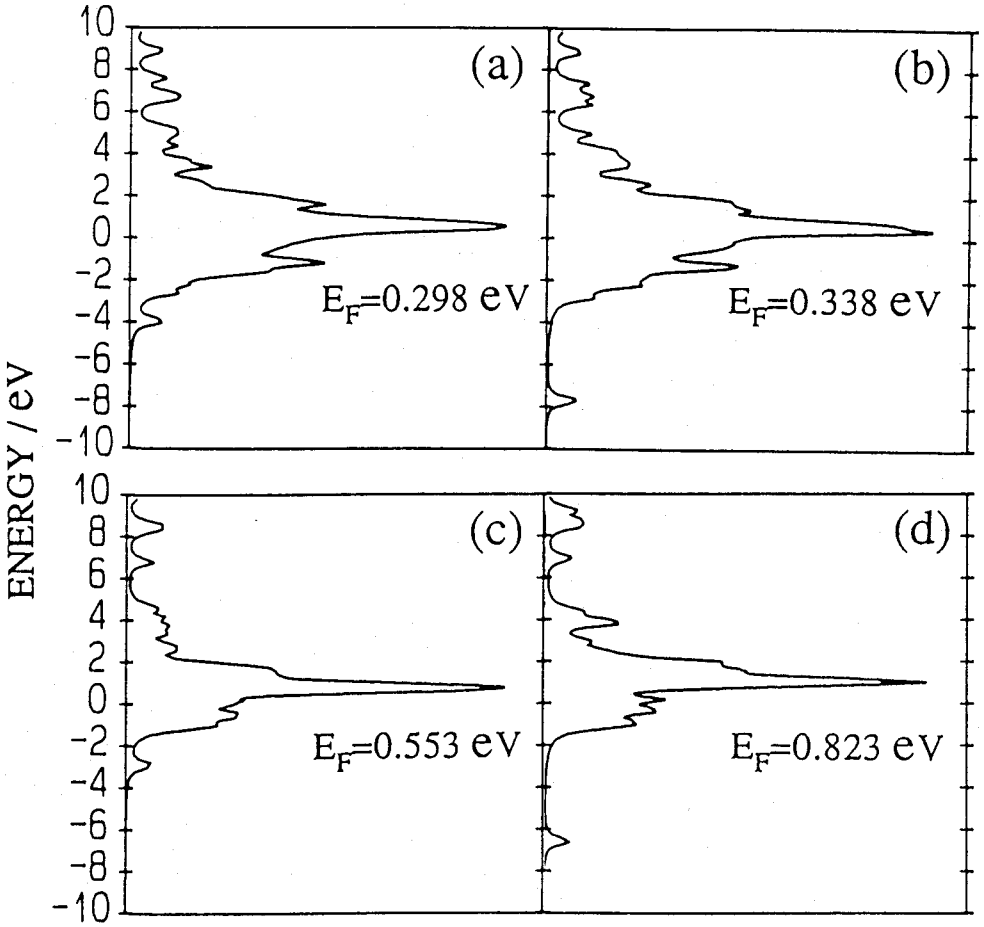

Fig. 5-2. Density of states for the model clusters of (a)A, (b)HA , (c)B and (d)HB.

where f_l is the degree of degeneracy and σ is the full-width-at-half-maximum(0.2 eV was adopted in Fig. 5-2).

Figures 5-2(a) and (b) show the DOS of the A and B clusters. In both figures, the DOS at near the highest occupied level , namely, the Fermi energy (E_F) is characterized by a narrow band consisting of two components corresponding to the Ni and La bands. The sharp partial DOS of the La 4f band (ca. 1eV) and most part of the La 5d band are located just above the Fermi level, and most part of the Ni 3d band lies just below the E_F. The small structure of the La band below the E_F in the energy range spanned by the Ni 3d band is characteristics of the La-Ni interaction. The Ni 4s and 4p bands and La 6s and 6p bands are broadly spread over a wide energy range.

The DOS of clusters with a hydrogen atom, HA and HB, are also shown in Fig. 5-2(b) and (d). Since the HA and HB clusters belong to the D_{2h} and C_{2v} symmetry groups, respectively, and the basis function from hydrogen is a 1s orbital, the direct effect of the interstitial hydrogen appear only in the a_{1g} representation for the HA cluster and the a_1 representation for the HB cluster.

The lowest level of the narrow band of the clusters with no hydrogen atom is the $24a_{1g}$ level (-3.930eV) for the A and the $27a_1$ level (-2.734eV) for the B cluster. The MO of these levels interacts with H1s orbital (-5.539eV) and contributes to formation of a hydrogen-metal bonding level located at -6.677eV ($24a_{1g}$) for HA and -6.457eV ($27a_1$) for HB. The large components of the

$24a_{1g}$ level for the HA cluster are H 1s(59%), Ni_I 4s(9%), Ni_I 3d(12%) and La 5d(5%), while those of the $27a_1$ level for the HB cluster are H 1s(62%), Ni_{II} 4s(11%), Ni_{II} 3d(10%) and La 5d(8%). The H 1s component of the hydrogen-metal bonding level shares a large proportion in comparison with that of other molecular orbital levels below the Fermi level in each clusters, so that the hydrogen -metal bond is characterized by this MO level.

The covalent bond strength and the contribution of atomic orbitals of the H atom and the surrounding metal atoms to the bond can be evaluated by the Mulliken's overlap population, which is listed in Table 5-1.

The overlap populations between H1s and Ni_I atomic orbitals in HA cluster take the small values, so that the H-Ni_I interaction is negligible.

The total overlap population for the H-Ni_{II} bond in the HA cluster shows a relatively large value of 0.22 as compared with 0.14 for the H-Ni_I total overlap population in the HB cluster, because the bonding contribution from the interaction between H 1s and Ni_{II} 4s and 4p in the HA cluster is larger than that in the HB cluster.

The H-La bond in these clusters is not formed as was suggested from the results of band structure calculation[32] of a β-phase $LaNi_5$ hydride, and the total overlap population of H-La bond in HA cluster takes the same small negative value, -0.07, as for HB cluster.

Table 5-1. Overlap populations between the interstitial hydrogen and surrounding metal atoms for two types of model clusters.

H - Ni_I			H - Ni_{II}			H - La		
	HA	HB		HA	HB		HA	HB
H 1s - Ni_I 3s	-0.03	—	H 1s - Ni_{II}3s	-0.01	-0.02	H 1s - La 5s	-0.02	-0.04
H 1s - Ni_I 3p	-0.02	—	H 1s - Ni_{II}3p	0.00	-0.02	H 1s - La 5p	-0.04	-0.06
H 1s - Ni_I 3d	+0.12	—	H 1s - Ni_{II}3d	+0.02	+0.11	H 1s - La 5d	+0.04	+0.11
H 1s - Ni_I 4s	+0.05	—	H 1s - Ni_{II}4s	-0.02	+0.02	H 1s - La 6s	-0.02	-0.03
H 1s - Ni_I 4p	+0.10	—	H 1s - Ni_{II}4p	0.00	+0.05	H 1s - La 6p	-0.03	-0.05
H atom - Ni_I atom	+0.22	—	H atom - Ni_{II} atom	-0.01	+0.14	H atom - La atom	-0.07	-0.07

It was found in both clusters as far as the bonding between hydrogen and the surrounding matal atoms is concerned that the bonding interaction was formed between hydrogen and the two nickel atoms (two Ni_{II} atoms in the HA cluster and two Ni_{I} atoms in the HB cluster) and that the antibonding interaction between hydrogen and the two La atoms. The Ni-H bonding interaction is found to be rather stronger in the HA cluster than that in the HB cluster.

From a view point of bonding nature between metal atoms, the covalency between metal atoms is weakened by the direct interaction between hydrogen and metal atoms, though the hydrogen-metal bond is simultaneously formed.

Table 5-2. gives the total overlap populations between metal atoms.

As a result of hydrogenation, decrease or no change in bond overlap population was found in both clusters. In the B cluster, change in overlap population for Ni_{II}-Ni_{II} and Ni_{II}-La bonds takes rather large negative values as compared with those for the other combination of atoms. In the case of Ni_{II}-Ni_{II} bond, Ni 3d-Ni 4p overlap population decreases with the occupation of hydrogen from a value of 0.18 to 0.00, and Ni 4s-Ni 4p overlap population decreases from a value of 0.21 to 0.16. In the case of Ni_{II}-La bond, overlap populations decrease in all combinations between La 5d, 6s, 6p and Ni 3d, 4s, 4p orbitals. The metal-metal bond is weakened as a result of decrease in overlap population of metal-

Table 5-2. Change in bond overlap populations between metal atoms resulting from hydrogenation.

	Total bond overlap population (/ bond)		Differences		Total bond overlap population (/ bond)		Differences
	(a) A	(b) HA	(b) - (a)		(c) B	(d) HB	(d) - (c)
Ni_I-Ni_{II}	0.41	0.38	-0.03	Ni_{II}-Ni_{II}	0.39	0.24	-0.15
Ni_I-La	0.35	0.32	-0.03	Ni_{II}-La	0.39	0.30	-0.09
Ni_{II}-La	0.27	0.27	0.00	La-La	0.50	0.46	-0.04
La-La	0.03	0.03	0.00				

metal bond and this affects the increase in total energy of the cluster. Thus, hydrogen prefers to occupy the A interstitial site rather than the B site as far as the metal-metal interaction is concerned. From the previous study[42] using cluster models with respect to the hydrogen-transition metal interaction, the formation of metallic hydrides accompanied by an endothermic or exothermic reaction respectively depends on weakening or strengthening the metal-metal bonds.

5.4 Conclusion

In our calculations of cluster models of 3f and 6m sites in the α-phase $LaNi_5$ hydride, hydrogen in the 3f site is more stable than in the 6m site from the view point of both the hydrogen-metal bonds and the metal-metal bonds. This calculation result is supported by the neutron inelastic scattering result that the hydrogen occupation of the 3f site is greater than that of the 6m site.[15]

It was also revealed by modeling the hydrogen sites of the $LaNi_5$ alloy that the electronic structure of local region of the alloy hydride system is closely related to its hydrogen absorption properties, so that the local electronic states of amorphous $LaNi_5$ alloy hydride appear to be calculated using cluster models of which the atomic configurations were determined by the information obtained from the EXAFS analyses described in the Chapter 1-4.

Summary

In this thesis, the local structure of the amorphous rare earth hydrogen storage alloy has been investigated, and the explanation of hydrogen absorption mechanisms of the alloys was attempted. The conclusions to be drawn from this work are as follows.

1. $LaNi_{5.0}$ amorphous alloys were found to have short range order that are very similar to those of the crystalline alloy. When the structural parameters of both amorphous and crystalline alloys were compared, it was revealed that the interatomic distances of some metal-metal pairs increased by amorphization. The decrease in hydrogen concentration caused by amorphization appears to be related to both distortions of hydrogen sites due to the increase in interatomic distances of metal-metal pairs and fluctuations of the size of the sites.

2. Judging from the change in the size of hydrogen sites during hydrogen absorption, hydrogen was found to occupy the sites, previously existed in the amorphous alloy, with optimum size to hydrogen atoms. The concentration of these sites in the amorphous alloy is less than that in the crystalline one, so that the decrease in the hydrogen concentration was observed in the amorphous alloy .

It was also found that the way of increase in interatomic distance with the concentration of hydrogen absorbed in the

$LaNi_{5.0}$ amorphous alloy is almost identical to that in the α-phase (low hydrogen density phase) of the crystalline alloy. It appears that amorphous alloys have a large resistance to pulverization because of minimal changes in interatomic distances with the concentration of hydrogen absorbed.

3. The difference in the hydrogen concentration of amorphous alloys prepared by reactive sputtering and conventional sputtering is considered to be due to the difference in the distribution of the size of the hydrogen sites. This difference strongly appears in the rate of hydrogen occupancy at the D3 site.

4. The local structure of an amorphous alloy prepared by evaporating was found to agree with that of an alloy obtained by conventional sputtering. It was suggested that the similarity in the local structures on both alloys reflects that in the hydrogen absorption characteristics.

5. From calculations on the electronic states of model clusters for the hydrogen sites in α-phase $LaNi_{5.0}$ alloy hydrides, it was revealed that hydrogen atoms occupied on the 6m and 3f sites bond with two Ni atoms and that the bonding force at the 3f site is much stronger than that at the 6m site. It was also shown that the bonding force of metal-metal pairs at the 6m site decreased due to

hydrogen occupation. This suggests that the instability of the clusters increases owing to the occupation of hydrogen in the 6m site.

It appeared that hydrogen preferred to occupy 3f site and that this preference was supported by the results from neutron inelastic scattering experiments.

References

1)J. H. N. van Vucht, F. A. Kuijpers and H. C. A. M. Bruning, *Philips Res. Rep.*, **25**(1970)133.

2)K. H. J. Buschow and H. H. Van Mal, *J. Less-Common Met.*, **29**, 203(1972).

3)M. Miyamoto, K. Yamaji and Y. Nakata, *J. Less-Common Met.*, **89**, 111(1983).

4)P. P. Turillon, *Less-Common Met.*, **74**, 322(1980).

5)J. R. van Beek, H. C. Donkersloot and J. J. G. Willems, *Power Source*, **10**, 317(1985).

6)G. Adachi, H. Nagai and J. Shiokawa, *J. Less-Common Met.*, **97**, L9(1984).

7)Y. Osumi, H. Suzuki, A. Kato, K. Oguro and M. Nakane, *Nippon Kagaku Kaisi*, **45**(1979).

8)H. Sakaguchi, N. Taniguchi, H. Seri, G. Adachi and J. Shiokawa, *J. Appl. Phys.*, **64**, 888(1988).

9)H. Sakaguchi, N. Taniguchi, H. Nagai, K. Niki, G. Adachi and J. Shiokawa, *J. Phys. Chem.*, **89**, 5550(1985).

10)C. Lartigue, A. Percheron-Guegan, J. C. Achard and J.L.Soubeyroux, *J. Less-Common Met.*, **113**(1985)127.

11)P. Thompson, J. J. Reilly, L. M. Corliss, J. M. Hastings and R. Hempelmann, *J. Phys. F:Met. Phys.*, **16**(1986)675.

12)C. Lartigue, A. Le. Bail and A. Percheron-Guegan, *J. Less-Common Met.*, **129**(1987)65.

13)J. L. Soubeyroux, A. Percheron-Guegan, and J. C. Achard, *J. Less-Common Met.*, **129**(1987)181.

14)D. Noreus, L. G. Olsson and P-E. Werner, *J. Phys. F: Met. Phys.*, 13(1983)715.

15)R. Hempelmann, D. Richter, G. Eckold, J. J. Rush, J. M. Rowe and M. Montoya, *J. Less-Common Met.*, **104**(1984)1.

16)B. K. Teo, *EXAFS : Basic Principles and Data Analysis*, Springer, Berlin, 1986.

17)A. Rosen, D. E. Ellis, H. Adachi and F. W. Averill, *J. Chem. Phys.*, **65**, 3629 (1976).

18)G. Adachi, H. Sakaguchi, K. Niki, H. Nagai, and J. Shiokawa, *Bull. Chem. Soc. Jpn.*, **58**, 885(1985).

19)H. Sakaguchi, H. Seri, and G. Adachi, *J. Phys. Chem.*, **94**, 5313(1990).

20)B. J. Tan, H. J. Klabunde, T. Tanaka, H. Kanai, and S. Yoshida, *J. Am. Chem. Soc.*, **110**, 5951(1988).

21)H. Yamashita, H. Mizutani, T. Tanaka, T. Funabiki, and S. Yoshida, *J. Non-Cryst. Solids*, **95&96**, 419(1987).

22)T. Tanaka, H. Yamashita, R. Tsuchitani, T. Funabiki, and S. Yoshida, *J. Chem. Soc.*, **84**, 2987(1988).

23)E. A. Stern, *Phys. Rev. B.*, **10**, 3027(1974).

24)C. A. Ashley, and S. Doniach, *Phys. Rev. B.*, **11**, 1279(1975).

25)P. A. Lee, and J. B. Pendry, *Phys. Rev. B.*, **11**, 2795(1975).

26)A. Taylor, *J. Inst. Met.*, **77**, 585(1950).

27)K. Levenberg, *Quarterly Appl. Math.*, **2**, 164(1944).

28)B. K. Teo, P. A. Lee, A. L. Simons, P. Eisenberger, and B. M. Kincaid, *J. Am. Chem. Soc.*, **99**, 3854(1977).

29)P. A. Lee, B. K. Teo, and A. L. Simons, *J. Am. Chem. Soc.*, **99**, 3856(1977).

30)T. Claeson, J. B. Boyce, P. W. Lowe, and T. H. Gaballe, *Phys. Rev. B.*, **29**, 4969(1984).

31)B. Lengeler, and P. Eisenberger, *Phys. Rev. B.*, **21**, 4507(1980).

32)M. Gupta, *J. Less-Common Met.*, **130**, 219(1987).

33)H. Hayakawa, K. Nomura, Y. Ishido, Y. Akiba, and S. Shin, *J. Less-Common Met.*, **143**, 315(1988).

34)J. Garcia, J. Bartolome, M. Sanchez del Rio, A. Marcelli, D. Fruchart and S. Miraglia, *Z. Phys. Chem.*, **163**, 279(1989).

35)R. J. Davis, S. M. Landry, J. A. Horsley and M. Boudart, *Phys. Rev. B*, **39**, 10580(1989).

36)D. G. Westlake, *J. Less-Common Met.*, **90**, 251(1983).

37)H. Sakaguchi, T. Tsujimoto and G. Adachi, *Chem. Mat.*, **5**, 6(1993).

38)V. P. Glazkov, A. V. Irodova, V. A. Somenkov, S. Sh. Shilstein, V. E. Antonov and E. G. Ponyatovsky, *Fiz. Tverd. Tela.*, **26**(1984)3261.

39)H. Adachi, M. Tukada and C. Satoko, *J. Phys. Soc. Jpn.*, **45**, 875(1978).

40)R. S. Mulliken, *J. Chem. Phys.*, **23**,1841(1955).

41)R. S. Mulliken, *J. Chem. Phys.*, **23**,1833(1955).

42)H. Adachi and S. Imoto, *J. Phys. Soc. Jpn.*, **46**, 1194(1979).

43)H. Adachi, S. Imoto, T. Tanabe and M. Tukada, *J. Phys. Soc. Jpn.*, **44**, 1039(1978).

Acknowledgment

The author is greatly indebted to Professor Dr. Gin-ya Adachi, Department of Applied Chemistry, Faculty of Engineering, Osaka University, for his invaluable suggestions, continuous guidance and hearty encouragement throughout this work.

The author is also indebted to Professor Dr. Hiroshi Yoneyama for his helpful comments and suggestions in the course of this thesis.

The author wishes to make a grateful acknowledgment to Dr. Hiroki Sakaguchi for his constant guidance and stimulating discussions.

The author is also very grateful to Associate Professor Dr. Ken-ichi Machida and Lecturer Dr. Nobuhito Imanaka for their helpful suggestions and heartfelt advice.

The author is deeply grateful to Professor Dr. Satohiro Yoshida, Department of Hydrocarbon Chemistry, Faculty of Engineering, Kyoto University and Professor Dr. Hiroyoshi Kanai Faculty of Living Science, Kyoto Prefectural University for their kind guidance in EXAFS experiments and analyses at the beginning of this work.

The author acknowledges to Professor Dr. Hirohiko Adachi and Dr. Isao Tanaka, Department of Metallurgy, Faculty of

Engineering, Kyoto University for their cordial guidance and helpful advice in the molecular orbital calculations.

The author's gratitude is expended to all the author's co-workers : Mr. Takaharu Tsuji, Mr. Hiroo Shirai, Mr. Eiji Yamamoto, Mr. Kazuhiro Nishioka, Mr. Hidenori Tanaka, Mr. Tetsuji Tsujimoto, Mr. Kiyoaki Moriuchi, Mr. Takuo Sugioka and Miss Noriko Waku for their helpful discussions and assistance.

Furthermore, many thanks are due to Dr. Nobuyuki Higashiyama and all the other members of the research group of Professor Dr. Gin-ya Adachi for their help and occasional discussions.

Finally, the author is particularly grateful to his father, the late Mr. Yasuo Suenobu, his mother, Mrs. Sachiko Suenobu, and his sister, Miss Keiko Suenobu for their perpetual support and encouragement.